https://doi.org/10.5194/esurf-2023-13
Preprint. Discussion started: 15 May 2023

Earth Surface Dynamics Discussions
Open Access
EGU

Long Runout Landslides with Associated Longitudinal Ridges in Iceland as Analogues of Martian Landforms.

Giulia Magnarini[1], Anya Champagne[2], Costanza Morino[3], Calvin Beck[4], Meven Philippe[5], Armelle Decaulne[6], Susan J. Conway[5]

[1]Natural History Museum, London, United Kingdom.
[2]Department of Earth Science and Engineering, Imperial College, London, United Kingdom.
[3]Université Savoie Mont Blanc, CNRS UMR 5204, Laboratoire Environnements, Dynamiques et Territoires de la Montagne, France.
[4]Normandie Université – UNICAEN - UNIROUEN, CNRS, UMR 6143 M2C, Laboratoire Morphodynamique Continentale et Côtière, Caen, France.
[5]Nantes Université – Université d'Angers – Le Mans Université, CNRS UMR 6112, Laboratoire de Planétologie et Géosciences, Nantes France.
[6]CNRS UMR 6554, Laboratoire Littoral - Environnement - Télédétection – Géomatique, Nantes, France

Correspondence to: Giulia Magnarini (giulia.magnarini@nhm.ac.uk)

Abstract. Much work has been done to study the behaviour of long runout landslides and their associated longitudinal ridges, yet the origin of the hypermobility of such landslides and the formation mechanism of longitudinal ridges are poorly understood. As terrestrial long runout landslides emplaced on glaciers commonly exhibit longitudinal ridges, the presence of these landforms has been used to infer the presence of ice on Mars, where hundreds of well-preserved long runout landslides with longitudinal ridges are found. However, the presence of the same landforms in regions where extensive glaciations did not occur, for instance, on the Moon and in the Atacama region on Earth, suggests that ice is not the only factor influencing the formation of long runout landslides with longitudinal ridges.

Iceland is a unique region for its high spatial density of well-preserved hypermobile large landslides with longitudinal ridges. Here, we compiled the first catalogue of Icelandic long runout landslides with longitudinal ridges and we compared them with martian long runout landslides with longitudinal ridges of similar length. Moreover, we present detailed morphological observations of the Dalvík landslide deposit, in the Tröllaskagi peninsula, Iceland and compare them with morphological observations of martian landslides.

Our results show that Icelandic long runout landslides share key features with martian analogue deposits, including splitting of longitudinal ridges and development of associated en-echelon features. Therefore, Icelandic long runout landslides with longitudinal ridges represent good analogues of martian landforms. Moreover, Iceland represents the ideal site to investigate these landforms at a regional scale and their link with ice retreat following the Late Glacial Maximum, which could also provide insights into martian paleoclimatic and paleoenvironmental conditions.

https://doi.org/10.5194/esurf-2023-13
Preprint. Discussion started: 15 May 2023

1 Introduction

Long runout landslides are hypermobile landslides that can have distinctive morphologies, such as longitudinal ridges, which are features visible at the surface of the deposit and extend parallel to the direction of movement (Figure 1). The hypermobility of long runout landslides is expressed by their horizontal runouts (L) that are significantly longer than their vertical drops (H). In the literature, the H/L ratio is used to describe the mobility of landslides, which for long runout landslides is significantly lower than 0.6 (e.g., Heim, 1932; Hsü, 1978; Legros, 2002).

Long runout landslides and their associated longitudinal ridges are ubiquitous in the Solar System (Beddingfield et al., 2020; Lucchitta, 1979; Schmidt et al., 2017; Singer et al., 2012), and their behaviour has been extensively studied (e.g., Davies and McSaveney, 2012; Harrison and Grimm, 2003; Legros, 2002; Lucas et al., 2014; Pudasaini and Miller, 2013; Vardoulakis, 2000; Voight and Faust, 1982), yet the origin of the hypermobility of such landslides and the formation mechanism of the longitudinal ridges are poorly understood. So far, two hypotheses have emerged: 1) the environment-dependent origin, in which environmental conditions, namely the presence of basal ice (De Blasio, 2011, 2014; Dufresne and Davies, 2009; Lucchitta, 1987; Mège and Bourgeois, 2011; Schmidt et al., 2017) and/or clays (Watkins et al., 2015), are a necessary condition for the development of long runout landslides and their associated longitudinal ridges. According to this hypothesis, low friction surfaces would favour tensional deformation of the sliding mass, by both longitudinal stretching and lateral spreading (De Blasio, 2011; Dufresne and Davies, 2009). Such tensile deformation would generate the longitudinal structures observed on the surface of long runout landslide deposit by the mechanism of necking, similarly to the tensile deformation that generates boudinage in tectonic context. 2) the environment-independent origin, in which the development of longitudinal ridges does not depend on the presence of a specific environmental condition and/or lithology (Magnarini et al., 2019, 2021a, 2021b). Magnarini et al. (2019) propose that longitudinal ridges that characterise terrestrial and planetary long runout landslides may be the expression of a mechanical instability that emerges within the flowing mass once a velocity threshold is surpassed, as observed in laboratory experiments on rapid granular flows (Forterre and Pouliquen, 2001). However, as this mechanism involves the generation of helicoidal convection cells within the moving landslide, it is contradicted by the evidence of the preservation of the slope stratigraphy within the final deposit, attributed to the lack of turbulence during the emplacement of long runout landslides (e.g., Dufresne et al., 2016; Johnson, 1978; Magnarini et al., 2021a; Shreve, 1968; Weidinger et al., 2014). To reconcile with field observations, Magnarini et al. (2021a) speculate on the existence of a vibration-assisted mechanism that would be able to produce the longitudinal pattern via mechanical instability yet maintain the internal structures.

As terrestrial long runout landslides emplaced on glaciers commonly exhibit longitudinal ridges (e.g., Dufresne et al., 2019; McSaveney, 1978), the presence of these landforms and associated morphologies has been used to infer the presence of ice on Mars (De Blasio, 2011; Gourronc et al., 2014; Lucchitta, 1979, 1987), where hundreds of well-preserved long runout landslides with longitudinal ridges are found. However, the presence of the same landforms and associated morphologies in regions where extensive glaciations did not occur, for instance, on the Moon (e.g., Boyce et al., 2020) and in the Atacama

https://doi.org/10.5194/esurf-2023-13
Preprint. Discussion started: 15 May 2023

region on Earth (Mather et al., 2014), suggests that ice is not the only factor influencing the formation of long runout landslides with longitudinal ridges.

On Earth, there are not as many well-preserved cases of long runout landslides with associated longitudinal ridges as there are on Mars. Such difference might suggest that longitudinal ridges in long runout landslides do not commonly form on our planet. However, more than one hundred landslides characterised by longitudinal ridges are easily identifiable in Iceland (e.g., Decaulne et al., 2016; Mercier et al., 2013), making it an exceptional region on Earth for its high spatial density of such landforms. The unique record of long runout landslides with longitudinal ridges in Iceland suggests that either longitudinal ridges are indeed common in long runout landslides on Earth, but their record is more easily lost on our planet; or conditions in Iceland, at the time of landslide formation, were optimal for the development of these landforms. The study of long runout landslides with longitudinal ridges in Iceland represents an opportunity to investigate the formation mechanisms of such hypermobile landslides and their possible link with past environmental conditions. A better understanding of the influence of climatic, geological, and environmental conditions in the development of hypermobile landslides will have implications for both terrestrial hazard assessment and reconstruction of extra-terrestrial paleo-environments.

In this study, we conducted a detailed survey of landslides in Iceland to identify and compile the first Icelandic catalogue of long runout landslides with longitudinal ridges. We compared the morphological parameters of Icelandic landslides with martian landslides that are similar in length. We present detailed morphological observations of one Icelandic case study, the Dalvík landslide, and we compare them with morphological observations of analogue martian landslide deposits. We show that Icelandic long runout landslides share similar morphometric values and diagnostic structures, such as longitudinal ridges, to those observed in martian long runout landslides. Therefore, we conclude that Icelandic long runout landslides with associated longitudinal ridges can be used as good analogues of martian landforms, similar to other elements of the Icelandic landscape and its associated mass-wasting processes (e.g., Conway et al., 2015, 2019; de Haas et al., 2015; Hartmann et al., 2003; Morino et al., 2019, 2023).

2 Data and Methods.

2.1 Icelandic long runout landslides.

In order to identify and map long runout landslides with longitudinal ridges in Iceland, we used available high-resolution satellite/aerial imagery from Google Earth Engine and the Icelandic Map website (https://www.map.is). In ArcGIS, we used digital elevation models (DEMs) provided by ArcticDEM (Porter et al. (2018); 2 m/px resolution) and their hillshade models to extrapolate landslide morphometric data (elevation drop and horizontal length; H and L, respectively, in Supplementary Table T1). In combination with the image-data, the hillshade was used to identify the furthest point of the headscarp and toe of the deposit so their elevation values could be extracted from the DEM.

We acquired drone imagery of one Icelandic landslide, near the town of Dalvík (I-Landslide ID 47 in Supplementary Table T1). We used 10 Ground Control Points (GCPs) in order to correctly georeference the drone images (Supplementary Table

https://doi.org/10.5194/esurf-2023-13
Preprint. Discussion started: 15 May 2023

T2), acquired by differential GPS and marked by 0.8x0.8 m square orange targets easily visible in the images. We obtained the latitude and longitude coordinates (WGS84) and the height above the ellipsoid of 10 locations, of which 8 on the landslide deposit and 2 on the slope adjacent the distal, frontal edge of the deposit (Figure 4), using a Leica dGPS GS09. We occupied the points for >5 minutes and post-processed the data using the permanent GPS station in Akureyri (AKUR run by LMI (Landmælingar Íslands)) 38 km away from the site. The resulting positions had errors much less than the error produced by inherent uncertainty in identifying the control points in the drone images (the worst position had a standard deviation of 2.4 cm in vertical position, yet this was typically 3 mm). We calculated the elevation above the geoid (i.e., elevation above sea level) using an online geoid calculator (GeoidEval). We built a digital elevation model (DEM; 4.65 cm/px resolution) and an orthoimage (2.38 cm/px resolution) of the Dalvík landslide using Agisoft Metashape (dataset provided in Magnarini et al. (2023)).

2.2 Martian long runout landslides.

We made use of the landslide inventory provided by Crosta et al. (2018) to select martian landslides with longitudinal ridges that are less than 5 km long (Supplementary Table T3), which is double the length of the longest Icelandic landslide considered in this study (I-Landslide ID 103; L = 2629 m). We added additional landslides with longitudinal ridges that are not found in the Crosta et al. (2018) inventory, found using high-resolution satellite imagery acquired by the ConTeXt (CTX) camera (6 m/px resolution; Malin et al. (2007)) and, where available, the High-Resolution Imaging Science Experiment (HiRISE) camera (nominal resolution 25 cm/px; McEwen et al. (2007)) on board the NASA Mars Reconnaissance Orbiter (MRO). In ArcGIS, we calculated the elevation drop (H) and measured the horizontal length (L) using the HRSC MOLA-Blended global DEM at 200 m/px resolution (Fergason et al., 2018). CTX images were used to identify the top of the headscarp and toe of the deposit so their elevation values could be extracted from the DEM.

We generated digital elevation models (DEMs) and orthoimages of four landslides (M-Landslide ID 31; M-Landslide ID 42; M-Landslide ID 46; M-Landslide ID 47) using CTX (Malin, 2007; Malin et al., 2007) image pairs (Supplementary Table T4). CTX-derived DEMs were generated using the USGS Integrated Software for Imagers and Spectrometers (ISIS) software and commercial image analysis software SOCET SET (Kirk et al., 2008). DEMs were vertically and horizontally controlled to Mars Orbital Laser Altimeter topographic data (Smith et al., 1999; Zuber et al., 1992). The resolution of DEMs and orthoimages are 20 m/pixel and 6 m/pixel, respectively. We estimated the vertical precision of the CTX-derived DEMs using the established method of Okubo (2010) (Supplementary Table T4).

3 Landslides in Iceland.

Paraglacial adjustment, that is the readjustment of glaciated landscapes to non-glacial conditions following deglaciation, is considered a critical cause of slope instability in high latitude environments (e.g., Ballantyne and Stone, 2004; Wyrwoll, 1977). According to the ‘exhaustion model’ (Ballantyne, 2002; Cruden and Hu, 1993), during the paraglacial period, the

https://doi.org/10.5194/esurf-2023-13
Preprint. Discussion started: 15 May 2023

occurrence of mass-wasting decreases exponentially over time after deglaciation. In Iceland, the occurrence of large landslides is attributed to ice retreat following the Last Glacial Maximum (LGM), either by the effect of glacial debuttressing or glacial rebound (e.g., Ballantyne, 2002; Coquin et al., 2015; Cossart et al., 2014; Fernández-Fernández et al., 2022; Saemundsson et al., 2022; Vick et al., 2021) or by pressurised water derived from glacial melting (Whalley et al., 1983). The ages available for large landslides in Iceland fit the paraglacial exhaustion model. Most of the dated landslides occurred in the first half of the Holocene (Coquin et al., 2015; Cossart et al., 2014; Decaulne et al., 2016; Mercier et al., 2013, 2017), consistent with the Icelandic landslide theory of Jónsson (1957), according to which landslide activity initiated shortly after the retreat of the ice sheet at the end of the LGM. However, out of more than a hundred of landslides, only a few have been dated (Decaulne et al., 2016; Mercier et al., 2013, 2017), and patterns of landslide occurrence following deglaciation are still debated (e.g., Cossart et al., 2014). Therefore, more data are needed to better constrain the relationship between the occurrence of large landslides and the effects of deglaciation.

Iceland has a unique high spatial density of well-preserved hypermobile large landslides with longitudinal ridges (Figure 2; Figure 3). This type of landslide is commonly found in the Tröllaskagi peninsula, in Northern-central Iceland (Figure 4). This region is constituted of Tertiary basalt lava flows alternated with weathered red vesicular basaltic rocks (paleosols) (Johannesson and Saemundsson, 1989; Saemundsson, 1980; Thordarson and Hoskuldsson, 2002), the latter considered weak layers within which slope failure planes could potentially develop (Jónsson, 1957; Mercier et al., 2013). Three landslides with longitudinal ridges have been dated: the Vatn landslide (I-landslide ID 69 in this work) is thought to have occurred between 11,400 and 10,790 cal. yr BP (Decaulne et al., 2016); the Höfðahólar landslide (I-landslide ID 118 in this work) is thought to have occurred between 10,200 and 7,975 cal. yr BP (Mercier et al., 2013); the Flókadalur landslide (I-landslide ID 57 in this work) is thought to have occurred between 15,577 ± 1455 - 11,002 ± 2778 cal. yr BP (Mercier et al., 2017).

3.1 The Dalvík landslide.

In this study, we investigated in the field a landslide located one kilometre northeast of the town of Dalvík, in the Tröllaskagi peninsula (Figure 4). The Dalvík landslide (I-landslide ID 47) is good example of a well-preserved long runout landslide with longitudinal ridges in Iceland. The landslide has a horizontal runout (L) of 1.210km and a vertical drop (H) of 0.480 km (Figure 1), resulting in a H/L ratio of 0.396.

Similarly to other long runout landslides, the edges of the accumulation zone are steep (on average about 30º slope), and about 15-25 m high (Figure 5d). The bedrock in the headscarp exposure shows typical alternation of Tertiary lava layers and red paleosols (Figure 5a, 5b). The landslide deposit sits on a sedimentary cover that has an undulating surface appearance (Figure 5c) and could be due to previous mass movements or glacial deposits. The zone of depletion is characterised by a toreva block (about 200 m long, 450 m wide, and 80 m high), while the zone of accumulation is composed of a debris apron about 750 m long. Boulders decimetre- to metre-size are found on the surface of the deposit. However, size sorting of boulders from proximal to distal area of the landslide seems not to occur.

https://doi.org/10.5194/esurf-2023-13
Preprint. Discussion started: 15 May 2023


Earth Surface Dynamics Discussions Open Access EGU

160 The debris apron is characterised by longitudinal ridges, which can be identified from both aerial/satellite images and ground photos. The longitudinal ridges occur across the entire length of the debris apron (Figure 6). At some locations, longitudinal ridges bifurcate (e.g., locations marked with a star in Figure 6; red arrowheads in Figure 13), forming two ridges commonly narrower than the parent ridge. Consequently, the number of longitudinal ridges increases from the proximal to the distal area of the apron. Transverse ridges appear only on the SW-side of the deposit.

165 In addition to longitudinal ridges, the Dalvík landslide exhibits other linear structures, superposed on, and broadly transverse to the longitudinal ridges (Figure 7). These linear structures appear to have en-echelon configuration. The en-echelon structures appear to be oblique to the longitudinal direction of the ridges. Towards the frontal edge of the deposit, the orientation of these linear structures changes and gradually becomes perpendicular to the extension of the ridges, which corresponds to the direction of movement of the landslide.

170 3.2 Catalogue of Icelandic long runout landslides with longitudinal ridges.

We compiled the first catalogue of Icelandic long runout landslides with longitudinal ridges (Supplementary Table T1). We included only landslides that have distinct longitudinal ridges and we omit those landslides for which the presence of longitudinal ridges was uncertain. Ridges were identified by their horizontal continuity in the downslope direction and their presence is evaluated using a top-view observation of the landslide deposit.

175 The horizontal length of the Icelandic landslides spans from 0.287 km (I-landslide ID 127) to 2.629 km (I-landslide ID 103). The H/L ratio of this set of Icelandic long runout landslides ranges from 0.149 (I-landslide ID 18) to 0.58 (I-landslide ID 42). The statistics of the morphometry of Icelandic landslides is summarised in Figure 12 and Figure 13.

Some of the landslides have their headscarps at the top of cliffs and mountains (e.g., I-landslide ID 8, ID 9 in Figure 3), whereas other cases develop from the mid/lower part of slopes (e.g., I-landslide ID 74, ID 88 in Figure 3). All the landslide

180 deposits are characterised by steep edges, typically about 20 m high. Not all landslides have a toreva block. Another characteristic found in some landslides is the presence of lateral levees that develop continuously from the depletion zone. In about the 80% of the cases, the deposit does not entirely reach the slope break at the base of the slope. The landslides often rest on inclined surface that connects the slope to the bottom of the valley (e.g., I-landslide ID 45, 69, 74, ID 115 in Figure 3 and the Dalvík landslide). In the case of absence of the connecting inclined surface, landslides extend beyond the slope break

185 at the base of the slope (e.g., I-landslide ID 8, ID 9 in Figure 3).

4 Landslides on Mars.

Geomorphological observations have been used to provide evidence of paraglacial periods on Mars (e.g., Gourronc et al., 2014; Jawin et al., 2018; Jawin and Head, 2021; Mège and Bourgeois, 2011), that immediately postdate glacial retreat. These are characterised by an assemblage of specific landforms that develop in response to ice removal, glacial unloading, and the

190 exposure of steep slopes and large sediment stores (e.g., Ballantyne, 2002). In Valles Marineris, structures diagnostic of

https://doi.org/10.5194/esurf-2023-13
Preprint. Discussion started: 15 May 2023

deep-seated gravitational slope deformation have been described (Gourronc et al., 2014; Mège and Bourgeois, 2011) and their development has been interpreted as the consequence of slope debuttressing and decohesion following the retreat of glaciers (Makowska et al., 2016; Mège and Bourgeois, 2011).

Mège and Bourgeois (2011) suggest that the large long runout landslides in Valles Marineris are the result of an advanced stage of paraglacial, deep-seated gravitational slope deformation that led to large-scale catastrophic slope failures. Moreover, Mège and Bourgeois (2011) and Gourronc et al. (2014) conclude that the long runout landslides in Valles Marineris are supraglacial landslides based on two observations: first, the emplacement on ice could explain the excessive runout of the landslides (e.g., De Blasio, 2011, 2014; Dufresne et al., 2019; Dufresne and Davies, 2009; Lucas et al., 2011, 2014; Shreve, 1966); second, the longitudinal ridges that characterise their deposits are considered a morphological signature of landslides emplaced on glaciers (De Blasio, 2011; Dufresne and Davies, 2009). However, Magnarini et al. (2019) argue that the presence of an icy surface is not necessary to develop longitudinal ridges in long runout landslides on Mars, which instead could develop from a mechanical instability imparted by high-velocity granular flow mechanisms.

4.1 Martian long runout landslides with longitudinal ridges.

In this work, we compiled a catalogue of martian long runout landslides less than 5 km long that exhibit longitudinal ridges (Supplementary Table T3, Figure 8, Figure 9, Figure 10), thus comparable to the length of Icelandic long runout landslides with longitudinal ridges. We only included long runout landslides that have distinct longitudinal ridges and we did not consider landslides where the presence of longitudinal ridges is uncertain. Moreover, we have excluded deposits with longitudinal ridges that do not have matching headscarps.

The horizontal length of the martian landslides included in the catalogue spans from 0.508 km (M-landslide ID 3) to 4.902 km (M-landslide ID 43). The H/L ratio of this set of martian long runout landslides ranges from 0.076 (M-landslide ID 14) to 0.468 (M-landslide ID 12). The statistics of the morphometry of small martian landslides is summarised in Figure 12 and Figure 13. Small-scale martian long runout landslides with longitudinal ridges are found between 38º N and 34º S. The largest concentration is found in the chaotic terrains east of Valles Marineris and in the channels and valleys that flow into Chryse Planitia. Other major clusters are found in Noctis Labyrinthus and north of Terra Cimmeria. Some of the landslides have their headscarps at the top of cliffs and mountains (e.g., in Figure 9a, 9b; Figure 10a, 10g), whereas other cases develop from the lower part of slopes (e.g., in Figure 9c; in Figure 10b, 10c, 10e, 10f, 10h). All the landslide deposits are characterised by steep edges, typically about 20-50 m high. Only about 20% of these landslides have a toreva block. Another typical characteristic is the presence of lateral levees that develop continuously from the depletion zone (e.g., Figure 11a). The debris aprons rest on sub-horizontal surfaces, either valley or crater floors. In only five cases (M-landslide ID 67, 71, 79, 102, 112), the deposit does not entirely reach the slope break at the base of the slope (e.g., in Figure 10b, 10e, 10f).

At 20 m/px resolution, CTX-derived DEMs are not able to resolve longitudinal ridges in small-scale (< 5 km long) landslides. Unfortunately, no HiRISE image pairs are available to generate DEM of the landslides included in this work. However, longitudinal ridges are visible in both CTX and HiRISE images across the entire length of the debris aprons.

https://doi.org/10.5194/esurf-2023-13
Preprint. Discussion started: 15 May 2023

Similarly to what we observed at the Dalvík landslide, longitudinal ridges split, generating two ridges from a parent ridge (Figure 11).

5 Morphometric and morphological comparison between Icelandic and martian long runout landslides with longitudinal ridges.

The gigantic, long runout landslides on Mars have attracted much interest, giving rise to a common commonly accepted belief that martian landslides are an order of magnitude larger than terrestrial landslides (e.g., Brunetti et al., 2014; Legros, 2002; Lucchitta, 1978, 1979; McEwen, 1989). However, the availability of higher resolution orbital imagery has shown the existence of martian long runout landslides that are smaller and similar in size to terrestrial long runout landslides (Crosta et al., 2018; Guimpier et al., 2021, 2022). Not only they share morphometric similarities, but also morphological structures: in addition to longitudinal ridges, they are all characterised by steep terminal edges; additionally, both the Icelandic and martian populations can develop lateral levees or toreva blocks, and have their headscarps either at the top of cliffs or at a mid-to-lower part of slopes. However, only five martian landslides do not entirely reach the slope break at the base of the slope, whereas more than 80% of the Icelandic landslide deposits rest on the inclined surface that connects the slope to the bottom of the valley.

In order to conduct a morphometric comparison between Icelandic and small-scale martian long runout landslides with associated longitudinal ridges (Figure 12), we selected a subgroup of martian landslides with $L < 2800$ m, in order to match the maximum length of the Icelandic landslides. The statistical analysis shows that Icelandic landslides have median and mean values of length (median= 1037 m; mean = 1150 m) and elevation drops (median = 317 m; mean = 337 m) lower than the martian subgroup of landslides (length: median = 1930 m; mean = 1803 m. Elevation: median = 527 m; mean = 536 m). It is interesting that, although the same length range is considered, the martian landslide subgroup shows cases that are characterised by higher elevation drops (Icelandic max elevation drop = 810 m; martian max elevation drop = 1071 m). However, the martian subgroup is constituted of 51 landslides, less than half the population of the Icelandic landslides (N = 129).

Such difference in the population number of landslides within an equal length range may be due to the fact that small-scale landslides on Mars do not form as readily as they do in Iceland; and/or that the martian record of small-scale landslides has been largely removed. The former suggests that the removed small-scale martian landslides were much older than the Icelandic landslides, therefore they have been subject to either erosion or burial for much a longer time span. In fact, we identified several deposits almost fully obliterated by sedimentary burial (Supplementary Figure S1a, S1b). Moreover, one of the best examples is found in Coprates Chasma, Valles Marineris, on Mars, where we found evidence of landslides with longitudinal ridges that have been partially buried and subsequently exhumed (Supplementary Figure S1c). Therefore, we suggest that the different population numbers reflect the removal of the geomorphological records of martian long runout landslides. Moreover, this also suggests that such lost record has not been replaced by recent long runout landslide

https://doi.org/10.5194/esurf-2023-13
Preprint. Discussion started: 15 May 2023

formation. The ages of large, long runout landslides (> 10 km long) in Valles Marineris span from 3.5 Gya to 50 Ma (Quantin et al., 2004; Hager and Schedl, 2017) and younger, small-scale landslides (< 2 km long) have been found to be less than 20 My old (Guimpier et al., 2021). According to these results, it appears that long runout landslides on Mars have been recurring throughout much of the martian history, suggesting that the formation mechanism of long runout landslides and their longitudinal ridges is persistent in time. However, the lack of much more recent deposits suggests that the mechanism favourable to their formation may have become unavailable on Mars, whereas in Iceland it has operated since the LGM (Decaulne et al., 2016; Mercier et al., 2017, 2013).

In the literature, the H/L ratio has been plotted against other parameters, such as length (Beddingfield et al., 2020; Johnson and Sori, 2020; Schmidt et al., 2017; Singer et al., 2012), elevation drop (Johnson and Campbell, 2017), and volume (Johnson and Campbell, 2017; Legros, 2002; Lucas et al., 2014; McEwen, 1989), in order to find possible correlations that could explain the hypermobility of long runout landslides. The H/L ratio is found to decrease with increasing volume. However, the physical significant of the H/L ratio has been questioned as its definition does not involve the displacement of the centre of gravity, the spreading of mass, or the role of the topography (e.g., Legros, 2002; Lucas et al., 2014).

The top panel of Figure 13 is a visual representation of the H/L ratio that characterises the population of the landslides that we have analysed in this study, and it aims to compare the main morphometric characteristics (namely length and elevation drop) between the Icelandic and martian landslide population. The plot shows that the H/L range that characterises the two landslide populations overlaps, and that is there is no distinct trend in the H/L ratio of the Icelandic and small-scale martian landslides. Sometimes length (L) is used as a proxy for the volume of landslides, when volume values are not available, even though it has been shown that it does not show the same correlation as that between H/L ratio and the volume (e.g., Johnson and Campbell, 2017; Legros, 2002; Lucas et al., 2014). The plot obtained for the Icelandic and martian landslide populations of this study shows a weak correlation between the two parameters, that is that the H/L ratio decreases with increasing length. Instead, the plot H/L ratio versus elevation drop seems to show a better correlation, only for the martian landslides: the H/L ratio increases with increasing fall heights. This trend was shown to also exist for large landslides on Earth, Mars, and Iapetus by Johnson and Campbell (2017) and confirmed by their numerical simulations.

5.1 Flow structures and behaviour of longitudinal ridges.

We observed longitudinal ridges bifurcating, thus splitting and developing two ridges from the parent ridge, in both the Dalvík landslide (Figure 6 and Supplementary Figure S2a, S2b) and small-scale martian landslides (Figure 11). The resulting new ridges are less wide. This process leads to an increase in the number of longitudinal ridges with distance. Similar behaviour has been described for the 63-km-long martian Coprates Labes landslide, in Valles Marineris, by Magnarini et al. (2019) (Supplementary Figure S2c, S2d). Therefore, the occurrence of ridge splitting seems to be scale-independent. However, in the Dalvík landslide, we do not observe the appearance of new, smaller ridges between two existing ridges, which is observed in the small-scale martian landslide ID 109 (Figure 11b). Similar ridge behaviour is observed in two other

https://doi.org/10.5194/esurf-2023-13
Preprint. Discussion started: 15 May 2023

martian landslides that are not included in the current selection, the landslide shown in Figure 11c, and the Coprates Labes landslide (Magnarini et al., 2019).

Lateral spreading of landslide deposits has been considered as an important factor controlling the behaviour of longitudinal ridges and the thickness of a landslide deposit (Magnarini et al., 2021b). Unconfined long runout landslides tend to spread laterally, causing the thinning of the deposit with distance and hence divergence of the longitudinal ridges. However, the existence of a scaling relationship between the thickness of the landslide and the spacing between the ridges (Magnarini et al., 2019, 2021a, b) implies that as the landslide thins while laterally spreading then the distance between the ridges has to decrease accordingly. Therefore, the scaling relationship is maintained by the splitting of parent ridges and also by the appearance of new smaller ridges between spreading longitudinal ridges (Magnarini et al., 2019).

The fact that the Dalvík landslide shows only the splitting of parent longitudinal ridges into two smaller ridges and does not show the appearance of new ridges between two existing ridges may be due to limited lateral spreading at Dalvík compared to the martian examples. Limited lateral spreading in turn limits the thickness reduction of the deposit and limits the space for new ridges to develop. Lateral spreading may be limited in Dalvík by: the basal surface over which the landslide moved not providing sufficiently low friction; the rheology of the landslide prevented it from spreading further laterally; or the landslide was not large enough, thus did not have enough kinetic energy to expand further. The latter proposed explanation may have support in the fact that the landslides in which we report the appearance of new ridges (in addition to ridge splitting) are all much larger than the Dalvík landslide.

Similarly to the Dalvík landslide, linear, en-echelon structures are seen in an 8-km-long martian landslide (e.g., Figure 14a, 16b) and have also been described in the 63-km-long Coprates Labes landslide by Magnarini et al. (2019) (Figure 14c, 14d). Similar linear structures superposed on longitudinal ridges were also described in the Sherman Glacier landslide deposit, Alaska, as ‘transverse fissures’ by Shreve (1966) and McSaveney (1978), in the Lamplugh landslide, Alaska, by Dufresne et al. (2019), and in the Iymek landslide, China, by Shi et al. (2022). Such linear structures have been interpreted as kinematic indicators, as they indicate the differential velocity of adjacent sections of the landslides during emplacement (e.g., Dufresne et al., 2019; Magnarini et al., 2019; McSaveney, 1978; Shreve, 1966).

In the Dalvík landslide, towards the frontal edge of the deposit, these linear structures change orientation and gradually become perpendicular to the direction of the ridges (Figure 7), which corresponds to the direction of movement of the landslide. The observed change in the orientation of the en-echelon structures may represent the expression of changing velocity during emplacement: the oblique configuration shows that different parts of the deposit were characterised by different velocities; and the transition to transverse configuration, i.e., perpendicular to the landslide movement direction, shows that different parts of the landslide progressively attained similar velocity. Given that the oblique-to-transverse transition occurs towards the terminus of the deposit, it may represent evidence of slowing down of the landslide. However, such transition does not seem to take place towards the terminal part of the martian landslide in Figure 16a and 16b, therefore, either a different interpretation is required or the martian landslide came to a halt in a different manner than the Dalvík landslide.

https://doi.org/10.5194/esurf-2023-13
Preprint. Discussion started: 15 May 2023

6 Conclusions.

We compile the first catalogue of long runout landslides with longitudinal ridges in Iceland (n=129) and an equivalent catalogue of small-scale (< 5 km long) landslides with longitudinal ridges on Mars (n=112). We measured length and drop height in both catalogues and found significant overlap between the populations. In addition to morphometric comparability, our morphological observations show that Icelandic long runout landslides share similar structure behaviours with martian analogue deposits, such as splitting of longitudinal ridges and development of en-echelon features. Therefore, Icelandic long runout landslides with longitudinal ridges represent good analogues of martian landforms. The large record of long runout landslides with longitudinal ridges emplaced after the Last Glacial Maximum in Iceland offers a unique opportunity to study the possible relation between the development of these landforms and glacial/paraglacial conditions. Unlocking this information will both contribute to tackling the challenges that current glaciated regions will face due to ongoing global warming and gain insights into martian paleoclimatic and paleoenvironmental conditions.

Data availability.

The standard data products for Mars used in the study are available from the NASA PDS. The shapefiles and topographic products generated for this work are provided through the data repository Figshare (Magnarini et al., 2023).

Author contribution.

GM: Conceptualisation, Investigation, Field work, Writing – Original draft.
AC: Investigation.
CM: Writing – Reviewing and Editing.
MP: Field work, Writing – Reviewing and Editing.
CB: Field work, Writing – Reviewing and Editing.
AD: Writing – Reviewing and Editing.
SJC: Resources, Investigation, Field work, Writing – Reviewing and Editing.

Competing interests.

One author is one of the editors of the special issue. The peer-review process was guided by an independent editor, and the authors have also no other competing interests to declare.

https://doi.org/10.5194/esurf-2023-13
Preprint. Discussion started: 15 May 2023

Acknowledgements.

GM gratefully acknowledges UKRI Science Technology Facilities Council (STFC) funding ST/V000799/1.
SJC is funded for her HiRISE work by the French space agency CNES. SJC, MP and CB are funded by the Agence Nationale de la Recherche in the framework of the project ANR-19-CE01-0010 PERMOLARDS.
We acknowledge the financial support from the Observatoire Sciences de l'Univers Nantes Atlantique (OSUNA).

References

Ballantyne, C. K.: A general model of paraglacial landscape response, The Holocene, 12, 371–376, https://doi.org/10.1191/0959683602hl553fa, 2002.

Ballantyne, C. K. and Stone, J. O.: The Beinn Alligin rock avalanche, NW Scotland: cosmogenic 10Be dating, interpretation and significance, The Holocene, 14, 448–453, https://doi.org/10.1191/0959683604hl720rr, 2004.

Beddingfield, C. B., Beyer, R. A., Singer, K. N., McKinnon, W. B., Runyon, K., Grundy, W., Stern, S. A., Bray, V., Dhingra, R., Moore, J. M., Ennico, K., Olkin, C. B., Schenk, P., Spencer, J. R., Weaver, H. A., and Young, L. A.: Landslides on Charon, Icarus, 335, 113383, https://doi.org/10.1016/j.icarus.2019.07.017, 2020.

Boyce, J. M., Mouginis-Mark, P., and Robinson, M.: The Tsiolkovskiy crater landslide, the moon: An LROC view, Icarus, 337, 113464, https://doi.org/10.1016/j.icarus.2019.113464, 2020.

Brunetti, M. T., Guzzetti, F., Cardinali, M., Fiorucci, F., Santangelo, M., Mancinelli, P., Komatsu, G., and Borselli, L.: Analysis of a new geomorphological inventory of landslides in Valles Marineris, Mars, Earth Planet. Sci. Lett., 405, 156–168, https://doi.org/10.1016/j.epsl.2014.08.025, 2014.

Conway, S. J., Balme, M. R., Kreslavsky, M. A., Murray, J. B., and Towner, M. C.: The comparison of topographic long profiles of gullies on Earth to gullies on Mars: A signal of water on Mars, Icarus, 253, 189–204, https://doi.org/10.1016/j.icarus.2015.03.009, 2015.

Conway, S. J., de Haas, T., and Harrison, T. N.: Martian gullies: a comprehensive review of observations, mechanisms and insights from Earth analogues, Geol. Soc. Lond. Spec. Publ., 467, 7–66, https://doi.org/10.1144/SP467.14, 2019.

Coquin, J., Mercier, D., Bourgeois, O., Cossart, E., and Decaulne, A.: Gravitational spreading of mountain ridges coeval with Late Weichselian deglaciation: impact on glacial landscapes in Tröllaskagi, northern Iceland, Quat. Sci. Rev., 107, 197–213, https://doi.org/10.1016/j.quascirev.2014.10.023, 2015.

Cossart, E., Mercier, D., Decaulne, A., Feuillet, T., Jónsson, H. P., and Sæmundsson, Þ.: Impacts of post-glacial rebound on landslide spatial distribution at a regional scale in northern Iceland (Skagafjörður), Earth Surf. Process. Landf., 39, 336–350, https://doi.org/10.1002/esp.3450, 2014.

https://doi.org/10.5194/esurf-2023-13
Preprint. Discussion started: 15 May 2023

Crosta, G. B., Frattini, P., Valbuzzi, E., and De Blasio, F. V.: Introducing a New Inventory of Large Martian Landslides, Earth Space Sci., 5, 89–119, https://doi.org/10.1002/2017EA000324, 2018.

Cruden, D. M. and Hu, X. Q.: Exhaustion and steady state models for predicting landslide hazards in the Canadian Rocky Mountains, Geomorphology, 8, 279–285, https://doi.org/10.1016/0169-555X(93)90024-V, 1993.

Davies, T. R. H. and McSaveney, M. J.: Mobility of long-runout rock avalanches, in: Landslides: Types, Mechanisms and Modeling, edited by: Stead, D. and Clague, J. J., Cambridge University Press, Cambridge, 50–58, https://doi.org/10.1017/CBO9780511740367.006, 2012.

De Blasio, F. V.: Landslides in Valles Marineris (Mars): A possible role of basal lubrication by sub-surface ice, Planet. Space Sci., 59, 1384–1392, https://doi.org/10.1016/j.pss.2011.04.015, 2011.

De Blasio, F. V.: Friction and dynamics of rock avalanches travelling on glaciers, Geomorphology, 213, 88–98, https://doi.org/10.1016/j.geomorph.2014.01.001, 2014.

Decaulne, A., Cossart, E., Mercier, D., Feuillet, T., Coquin, J., and Jónsson, H. P.: An early Holocene age for the Vatn landslide (Skagafjörður, central northern Iceland): Insights into the role of postglacial landsliding on slope development, The Holocene, 26, 1304–1318, https://doi.org/10.1177/0959683616638432, 2016.

Dufresne, A. and Davies, T. R.: Longitudinal ridges in mass movement deposits, Geomorphology, 105, 171–181, https://doi.org/10.1016/j.geomorph.2008.09.009, 2009.

Dufresne, A., Bösmeier, A., and Prager, C.: Sedimentology of rock avalanche deposits – Case study and review, Earth-Sci. Rev., 163, 234–259, https://doi.org/10.1016/j.earscirev.2016.10.002, 2016.

Dufresne, A., Wolken, G. J., Hibert, C., Bessette-Kirton, E. K., Coe, J. A., Geertsema, M., and Ekström, G.: The 2016 Lamplugh rock avalanche, Alaska: deposit structures and emplacement dynamics, Landslides, 16, 2301–2319, https://doi.org/10.1007/s10346-019-01225-4, 2019.

Fergason, L. R., Hare, T. M., and Laura, J.: HRSC and MOLA Blended Digital Elevation Model at 200m v2. Astrogeology PDS Annex, U.S. Geological Survey., 2018.

Fernández-Fernández, J. M., Etzelmüller, B., Morino, C., and Sæmundsson, Þ.: Iceland, in: Periglacial Landscapes of Europe, edited by: Oliva, M., Nývlt, D., and Fernández-Fernández, J. M., Springer International Publishing, Cham, 427–473, https://doi.org/10.1007/978-3-031-14895-8_15, 2022.

Forterre, Y. and Pouliquen, O.: Longitudinal Vortices in Granular Flows, Phys. Rev. Lett., 86, 5886–5889, https://doi.org/10.1103/PhysRevLett.86.5886, 2001.

https://doi.org/10.5194/esurf-2023-13
Preprint. Discussion started: 15 May 2023

Gourronc, M., Bourgeois, O., Mège, D., Pochat, S., Bultel, B., Massé, M., Le Deit, L., Le Mouélic, S., and Mercier, D.: One million cubic kilometers of fossil ice in Valles Marineris: Relicts of a 3.5Gy old glacial landsystem along the Martian equator, Geomorphology, 204, 235–255, https://doi.org/10.1016/j.geomorph.2013.08.009, 2014.

Guimpier, A., Conway, S. J., Mangeney, A., Lucas, A., Mangold, N., Peruzzetto, M., Pajola, M., Lucchetti, A., Munaretto, G., Sæmundsson, T., Johnsson, A., Le Deit, L., Grindrod, P., Davis, J., Thomas, N., and Cremonese, G.: Dynamics of recent landslides (<20 My) on Mars: Insights from high-resolution topography on Earth and Mars and numerical modelling, Planet. Space Sci., 206, 105303, https://doi.org/10.1016/j.pss.2021.105303, 2021.

Guimpier, A., Conway, S. J., Pajola, M., Lucchetti, A., Simioni, E., Re, C., Noblet, A., Mangold, N., Thomas, N., and Cremonese, G.: Pre-landslide topographic reconstruction in Baetis Chaos, mars using a CaSSIS Digital Elevation Model, Planet. Space Sci., 218, 105505, https://doi.org/10.1016/j.pss.2022.105505, 2022.

de Haas, T., Hauber, E., Conway, S. J., van Steijn, H., Johnsson, A., and Kleinhans, M. G.: Earth-like aqueous debris-flow activity on Mars at high orbital obliquity in the last million years, Nat. Commun., 6, 7543, https://doi.org/10.1038/ncomms8543, 2015.

Hager, A. and Schedl, A. D.: Classification and Ages of Landslides Within Valles Marineris, 48th Lunar and Planetary Science Conference, event-title: 48th Annual Lunar and Planetary Science ConferenceADS Bibcode: 2017LPI....48.2076H, 2076, 2017.

Harrison, K. P. and Grimm, R. E.: Rheological constraints on martian landslides, Icarus, 163, 347–362, https://doi.org/10.1016/S0019-1035(03)00045-9, 2003.

Hartmann, W. K., Thorsteinsson, T., and Sigurdsson, F.: Martian hillside gullies and icelandic analogs, Icarus, 162, 259–277, https://doi.org/10.1016/S0019-1035(02)00065-9, 2003.

Heim, A.: Der Bergsturz und Menschenleben, Fretz und Wasmuth Verlag, Zurich, 218 pp., 1932.

Hsü, K. J.: Albert Heim: Observations on Landslides and Relevance to Modern Interpretations, in: Developments in Geotechnical Engineering, vol. 14, Elsevier, 71–93, https://doi.org/10.1016/B978-0-444-41507-3.50009-X, 1978.

Jawin, E. R. and Head, J. W.: Patterns of late Amazonian deglaciation from the distribution of martian paraglacial features, Icarus, 355, 114117, https://doi.org/10.1016/j.icarus.2020.114117, 2021.

Jawin, E. R., Head, J. W., and Marchant, D. R.: Transient post-glacial processes on Mars: Geomorphologic evidence for a paraglacial period, Icarus, 309, 187–206, https://doi.org/10.1016/j.icarus.2018.01.026, 2018.

Johannesson, H. and Saemundsson, K.: Geological map of Iceland, 1:500000, Bedrock geology, 1989.

Johnson, B.: Blackhawk Landslide, California, U.S.A., in: Developments in Geotechnical Engineering, vol. 14, Elsevier, 481–504, https://doi.org/10.1016/B978-0-444-41507-3.50022-2, 1978.

https://doi.org/10.5194/esurf-2023-13
Preprint. Discussion started: 15 May 2023

Johnson, B. C. and Campbell, C. S.: Drop Height and Volume Control the Mobility of Long-Runout Landslides on the Earth and Mars, Geophys. Res. Lett., 44, 12,091-12,097, https://doi.org/10.1002/2017GL076113, 2017.

Johnson, B. C. and Sori, M. M.: Landslide Morphology and Mobility on Ceres Controlled by Topography, J. Geophys. Res. Planets, 125, e2020JE006640, https://doi.org/10.1029/2020JE006640, 2020.

Jónsson, Ó.: Skriðuföll og snjóflóð, Bókaútgafan Norðri, 1, 141, 1957.

Kirk, R. L., Howington-Kraus, E., Rosiek, M. R., Anderson, J. A., Archinal, B. A., Becker, K. J., Cook, D. A., Galuszka, D. M., Geissler, P. E., Hare, T. M., Holmberg, I. M., Keszthelyi, L. P., Redding, B. L., Delamere, W. A., Gallagher, D., Chapel, J. D., Eliason, E. M., King, R., and McEwen, A. S.: Ultrahigh resolution topographic mapping of Mars with MRO HiRISE stereo images: Meter-scale slopes of candidate Phoenix landing sites, J. Geophys. Res. Planets, 113, https://doi.org/10.1029/2007JE003000, 2008.

Legros, F.: The mobility of long-runout landslides, Eng. Geol., 63, 301–331, https://doi.org/10.1016/S0013-7952(01)00090-4, 2002.

Lucas, A., Mangeney, A., Mège, D., and Bouchut, F.: Influence of the scar geometry on landslide dynamics and deposits: Application to Martian landslides, J. Geophys. Res. Planets, 116, https://doi.org/10.1029/2011JE003803, 2011.

Lucas, A., Mangeney, A., and Ampuero, J. P.: Frictional velocity-weakening in landslides on Earth and on other planetary bodies, Nat. Commun., 5, 3417, https://doi.org/10.1038/ncomms4417, 2014.

Lucchitta, B. K.: A large landslide on Mars, GSA Bull., 89, 1601–1609, https://doi.org/10.1130/0016-7606(1978)89<1601:ALLOM>2.0.CO;2, 1978.

Lucchitta, B. K.: Landslides in Valles Marineris, Mars, J. Geophys. Res. Solid Earth, 84, 8097–8113, https://doi.org/10.1029/JB084iB14p08097, 1979.

Lucchitta, B. K.: Valles Marineris, Mars: Wet debris flows and ground ice, Icarus, 72, 411–429, https://doi.org/10.1016/0019-1035(87)90183-7, 1987.

Magnarini, G., Mitchell, T. M., Grindrod, P. M., Goren, L., and Schmitt, H. H.: Longitudinal ridges imparted by high-speed granular flow mechanisms in martian landslides, Nat. Commun., 10, 4711, https://doi.org/10.1038/s41467-019-12734-0, 2019.

Magnarini, G., Mitchell, T. M., Goren, L., Grindrod, P. M., and Browning, J.: Implications of longitudinal ridges for the mechanics of ice-free long runout landslides, Earth Planet. Sci. Lett., 574, 117177, https://doi.org/10.1016/j.epsl.2021.117177, 2021a.

https://doi.org/10.5194/esurf-2023-13
Preprint. Discussion started: 15 May 2023

Magnarini, G., Mitchell, T. M., Grindrod, P. M., Schmitt, H. H., and Petro, N. E.: Scaling Relationship Between the Wavelength of Longitudinal Ridges and the Thickness of Long Runout Landslides on the Moon, J. Geophys. Res. Planets, 126, e2021JE006922, https://doi.org/10.1029/2021JE006922, 2021b.

Magnarini, G., Champagne, A., Morino, C., Beck, C., Philippe, M., and Conway, S. J.: Long Runout Landslides with Longitudinal Ridges in Iceland as Analogues of Martian Landforms [Dataset], https://doi.org/10.6084/m9.figshare.22333036.v1, 2023.

Makowska, M., Mège, D., Gueydan, F., and Chéry, J.: Mechanical conditions and modes of paraglacial deep-seated gravitational spreading in Valles Marineris, Mars, Geomorphology, 268, 246–252, https://doi.org/10.1016/j.geomorph.2016.06.011, 2016.

Malin, M.: MRO CONTEXT CAMERA EXPERIMENT DATA RECORD LEVEL 0 V1.0, https://doi.org/10.17189/1520266, 2007.

Malin, M. C., Bell III, J. F., Cantor, B. A., Caplinger, M. A., Calvin, W. M., Clancy, R. T., Edgett, K. S., Edwards, L., Haberle, R. M., James, P. B., Lee, S. W., Ravine, M. A., Thomas, P. C., and Wolff, M. J.: Context Camera Investigation on board the Mars Reconnaissance Orbiter, J. Geophys. Res. Planets, 112, https://doi.org/10.1029/2006JE002808, 2007.

Mather, A. E., Hartley, A. J., and Griffiths, J. S.: The giant coastal landslides of Northern Chile: Tectonic and climate interactions on a classic convergent plate margin, Earth Planet. Sci. Lett., 388, 249–256, https://doi.org/10.1016/j.epsl.2013.10.019, 2014.

McEwen, A. S.: Mobility of large rock avalanches: Evidence from Valles Marineris, Mars, Geology, 17, 1111–1114, https://doi.org/10.1130/0091-7613(1989)017<1111:MOLRAE>2.3.CO;2, 1989.

McEwen, A. S., Eliason, E. M., Bergstrom, J. W., Bridges, N. T., Hansen, C. J., Delamere, W. A., Grant, J. A., Gulick, V. C., Herkenhoff, K. E., Keszthelyi, L., Kirk, R. L., Mellon, M. T., Squyres, S. W., Thomas, N., and Weitz, C. M.: Mars Reconnaissance Orbiter's High Resolution Imaging Science Experiment (HiRISE), J. Geophys. Res. Planets, 112, https://doi.org/10.1029/2005JE002605, 2007.

McSaveney, M. J.: Chapter 6 - Sherman Glacier Rock Avalanche, Alaska, U.S.A., in: Developments in Geotechnical Engineering, vol. 14, edited by: Voight, B., Elsevier, 197–258, https://doi.org/10.1016/B978-0-444-41507-3.50014-3, 1978.

Mège, D. and Bourgeois, O.: Equatorial glaciations on Mars revealed by gravitational collapse of Valles Marineris wallslopes, Earth Planet. Sci. Lett., 310, 182–191, https://doi.org/10.1016/j.epsl.2011.08.030, 2011.

Mercier, D., Cossart, E., Decaulne, A., Feuillet, T., Jónsson, H. P., and Sæmundsson, Þ.: The Höfðahólar rock avalanche (sturzström): Chronological constraint of paraglacial landsliding on an Icelandic hillslope, The Holocene, 23, 432–446, https://doi.org/10.1177/0959683612463104, 2013.

https://doi.org/10.5194/esurf-2023-13
Preprint. Discussion started: 15 May 2023

Mercier, D., Coquin, J., Feuillet, T., Decaulne, A., Cossart, E., Jónsson, H. P., and Sæmundsson, Þ.: Are Icelandic rock-slope failures paraglacial? Age evaluation of seventeen rock-slope failures in the Skagafjörður area, based on geomorphological stacking, radiocarbon dating and tephrochronology, Geomorphology, 296, 45–58, https://doi.org/10.1016/j.geomorph.2017.08.011, 2017.

Morino, C., Conway, S. J., Sæmundsson, Þ., Helgason, J. K., Hillier, J., Butcher, F. E. G., Balme, M. R., Jordan, C., and Argles, T.: Molards as an indicator of permafrost degradation and landslide processes, Earth Planet. Sci. Lett., 516, 136–147, https://doi.org/10.1016/j.epsl.2019.03.040, 2019.

Morino, C., Conway, S., Philippe, M., Peignaux, C., Svennevig, K., Lucas, A., Noblet, A., Roberti, G., Butcher, F., and Collins-May, J.: Permafrost molards as an analogue for ejecta-ice interactions at Hale Crater, Mars, Icarus, 391, 115363, https://doi.org/10.1016/j.icarus.2022.115363, 2023.

Okubo, C. H.: Structural geology of Amazonian-aged layered sedimentary deposits in southwest Candor Chasma, Mars, Icarus, 207, 210–225, https://doi.org/10.1016/j.icarus.2009.11.012, 2010.

Porter, C., Morin, P., Howat, I., Noh, M.-J., Bates, B., Peterman, K., Keesey, S., Schlenk, M., Gardiner, J., Tomko, K., Willis, M., Kelleher, C., Cloutier, M., Husby, E., Foga, S., Nakamura, H., Platson, M., Wethington, M., Williamson, C., Bauer, G., Enos, J., Arnold, G., Kramer, W., Becker, P., Doshi, A., D'Souza, C., Cummens, P., Laurier, F., and Bojesen, M.: ArcticDEM, https://doi.org/10.7910/DVN/OHHUKH, 2018.

Pudasaini, S. P. and Miller, S. A.: The hypermobility of huge landslides and avalanches, Eng. Geol., 157, 124–132, https://doi.org/10.1016/j.enggeo.2013.01.012, 2013.

Quantin, C., Allemand, P., Mangold, N., and Delacourt, C.: Ages of Valles Marineris (Mars) landslides and implications for canyon history, Icarus, 172, 555–572, https://doi.org/10.1016/j.icarus.2004.06.013, 2004.

Saemundsson, K.: Outlines of the geology of Iceland, Jökull, 29, 7–28, 1980.

Saemundsson, P., Morino, C., and Conway, S. J.: 5.22 - Mass-Movements in Cold and Polar Climates, in: Treatise on Geomorphology (Second Edition), edited by: Shroder, J. (Jack) F., Academic Press, Oxford, 350–370, https://doi.org/10.1016/B978-0-12-818234-5.00117-6, 2022.

Schmidt, B. E., Hughson, K. H. G., Chilton, H. T., Scully, J. E. C., Platz, T., Nathues, A., Sizemore, H., Bland, M. T., Byrne, S., Marchi, S., O'Brien, D. P., Schorghofer, N., Hiesinger, H., Jaumann, R., Pasckert, J. H., Lawrence, J. D., Buzckowski, D., Castillo-Rogez, J. C., Sykes, M. V., Schenk, P. M., DeSanctis, M.-C., Mitri, G., Formisano, M., Li, J.-Y., Reddy, V., LeCorre, L., Russell, C. T., and Raymond, C. A.: Geomorphological evidence for ground ice on dwarf planet Ceres, Nat. Geosci., 10, 338–343, https://doi.org/10.1038/ngeo2936, 2017.

https://doi.org/10.5194/esurf-2023-13
Preprint. Discussion started: 15 May 2023

Shi, A.-W., Wang, Y.-F., Cheng, Q.-G., Lin, Q.-W., Li, T.-H., and Wünnemann, B.: The largest rock avalanche in China at Iymek, Eastern Pamir, and its spectacular emplacement landscape, Geomorphology, 108521, https://doi.org/10.1016/j.geomorph.2022.108521, 2022.

Shreve, R. L.: Sherman Landslide, Alaska, Science, 154, 1639–1643, https://doi.org/10.1126/science.154.3757.1639, 1966.

Shreve, R. L.: The Blackhawk landslide, Geological Society of America, Boulder, Colo, 47 pp., 1968.

Singer, K. N., McKinnon, W. B., Schenk, P. M., and Moore, J. M.: Massive ice avalanches on Iapetus mobilized by friction reduction during flash heating, Nat. Geosci., 5, 574–578, https://doi.org/10.1038/ngeo1526, 2012.

Smith, D. E., Zuber, M. T., Solomon, S. C., Phillips, R. J., Head, J. W., Garvin, J. B., Banerdt, W. B., Muhleman, D. O., Pettengill, G. H., Neumann, G. A., Lemoine, F. G., Abshire, J. B., Aharonson, O., David, C., Brown, Hauck, S. A., Ivanov, A. B., McGovern, P. J., Zwally, H. J., and Duxbury, T. C.: The Global Topography of Mars and Implications for Surface Evolution, Science, 284, 1495–1503, https://doi.org/10.1126/science.284.5419.1495, 1999.

Thordarson, T. and Hoskuldsson, A.: Iceland (Classic Geology in Europe 3), Terra Publishing (UK), 200 pp., 2002.

Vardoulakis: Catastrophic landslides due to frictional heating of the failure plane, Mech. Cohesive-Frict. Mater., 5, 443–467, https://doi.org/10.1002/1099-1484(200008)5:6<443::AID-CFM104>3.0.CO;2-W, 2000.

Vick, L. M., Mikkelsen, M., Corner, G. D., Kjellman, S. E., Trønnes, L., Hormes, A., Allaart, L., and Bergh, S. G.: Evolution and temporal constraints of a multiphase postglacial rock slope failure, Geomorphology, 398, 108069, https://doi.org/10.1016/j.geomorph.2021.108069, 2021.

Voight, B. and Faust, C.: Frictional heat and strength loss in some rapid landslides, Géotechnique, 32, 43–54, https://doi.org/10.1680/geot.1982.32.1.43, 1982.

Watkins, J. A., Ehlmann, B. L., and Yin, A.: Long-runout landslides and the long-lasting effects of early water activity on Mars, Geology, 43, 107–110, https://doi.org/10.1130/G36215.1, 2015.

Weidinger, J. T., Korup, O., Munack, H., Altenberger, U., Dunning, S. A., Tippelt, G., and Lottermoser, W.: Giant rockslides from the inside, Earth Planet. Sci. Lett., 389, 62–73, https://doi.org/10.1016/j.epsl.2013.12.017, 2014.

Whalley, W. B., Douglas, G. R., and Jonsson, A.: The Magnitude and Frequency of Large Rockslides in Iceland in the Postglacial, Geogr. Ann. Ser. Phys. Geogr., 65, 99–110, https://doi.org/10.2307/520724, 1983.

Wyrwoll, K. H.: Causes of rock-slope failure in a cold area: Labrador-Ungava., in: Reviews in Engineering Geology: Vol. 3 - Landslides., vol. 3, Geological Society of America, 59–67, 1977.

https://doi.org/10.5194/esurf-2023-13
Preprint. Discussion started: 15 May 2023

550 Zuber, M. T., Smith, D. E., Solomon, S. C., Muhleman, D. O., Head, J. W., Garvin, J. B., Abshire, J. B., and Bufton, J. L.: The Mars Observer laser altimeter investigation, J. Geophys. Res. Planets, 97, 7781–7797, https://doi.org/10.1029/92JE00341, 1992.

555

560

565

https://doi.org/10.5194/esurf-2023-13
Preprint. Discussion started: 15 May 2023

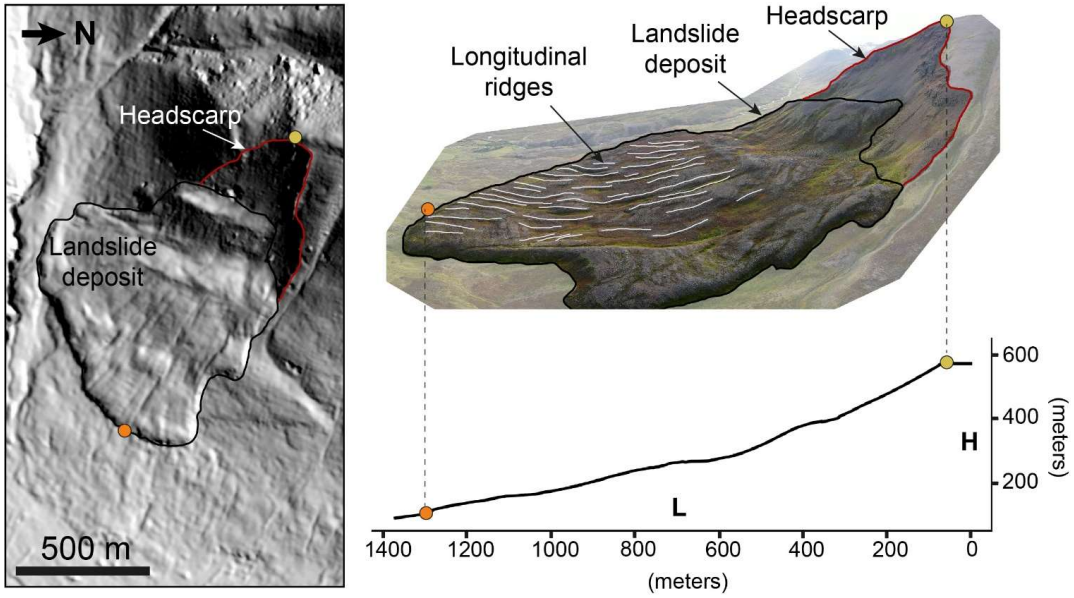

Figure 1: Example of a terrestrial long runout landslide with longitudinal ridges. The red line shows the headscarp of the landslide. The black line shows the extent of the landslide deposit. The white lines show the longitudinal ridges that mark the landslide deposit and extend parallel to the direction of the movement. The yellow and orange dots represent the highest point of the headscarp and the lowest point of the deposit, respectively; these locations are used to derive the elevation drop (H) and the horizontal extent (L) of the landslide. Left panel shows the hillshade model of the Dalvík landslide obtained from the 2 m/px resolution ArcticDEM (Porter et al., 2018). The right panel shows a photomosaic from drone imagery of the Dalvík landslide and its longitudinal topographic profile.

https://doi.org/10.5194/esurf-2023-13
Preprint. Discussion started: 15 May 2023

Earth Surface Dynamics Discussions
Open Access
EGU

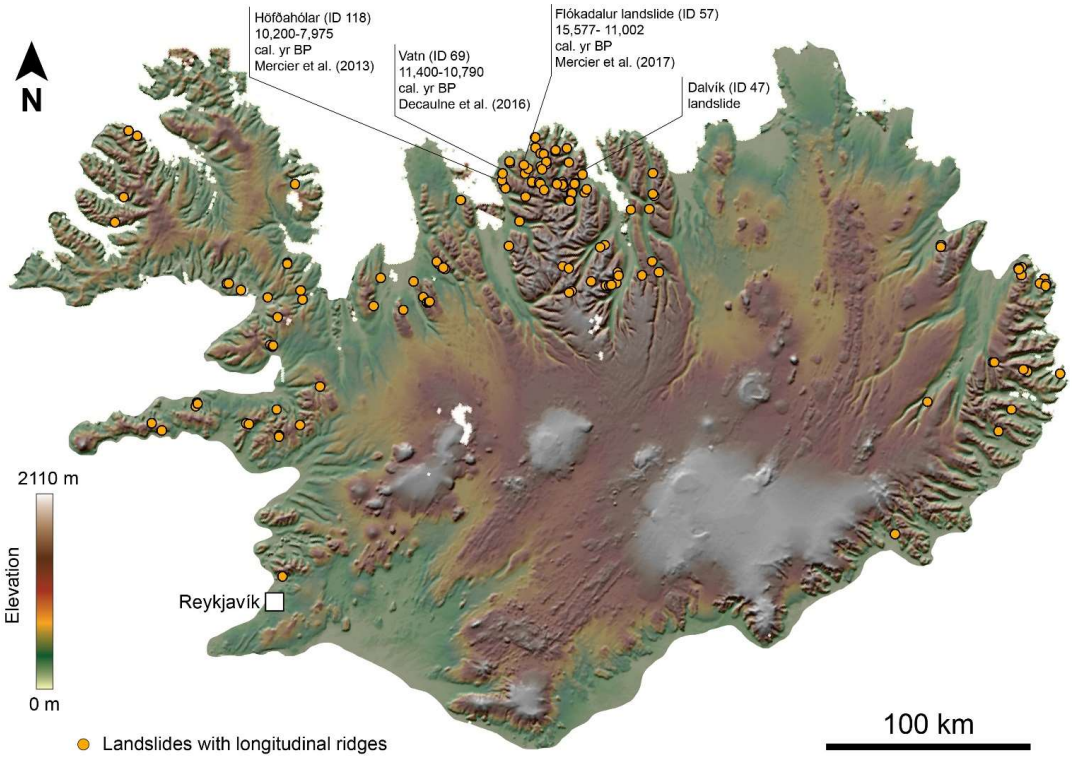

Figure 2: Distribution of long runout landslides with longitudinal ridges in Iceland. The yellow dots represent locations of 129 long runout landslides with longitudinal ridges, which geographic coordinates are given in Supplementary Table T1. The map shows the location of the three landslides with longitudinal ridges that have been dated by previous work and the location of the Dalvík landslide, investigated in this work. Base map is the hillshaded and colour-keyed 500 m/px resolution ArcticDEM (Porter et al., 2018).

https://doi.org/10.5194/esurf-2023-13
Preprint. Discussion started: 15 May 2023

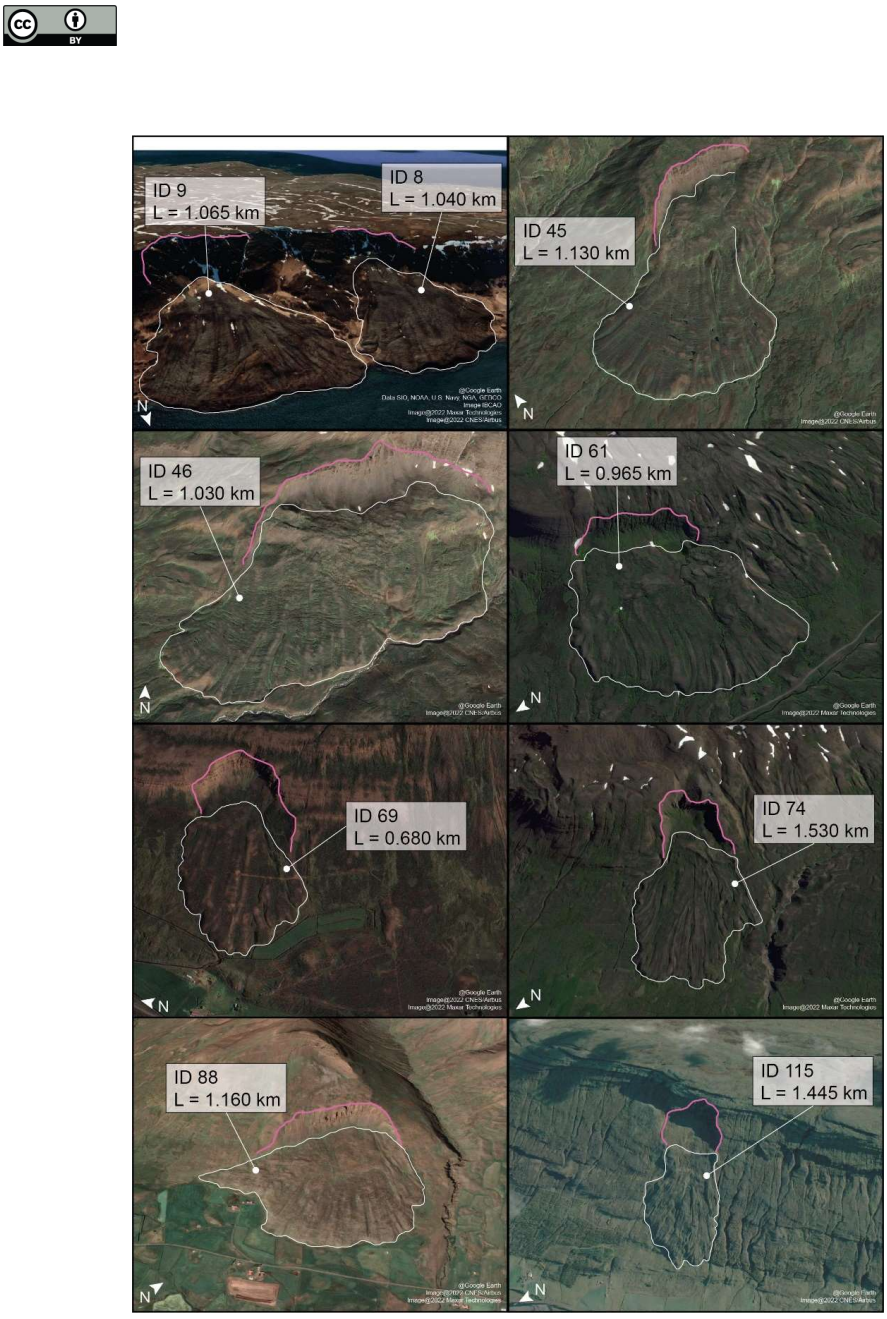

585 **Figure 3: Examples of long runout landslides with ridges in Iceland.** The white lines identify the landslide deposits and the pink lines identify the headscarps. For each landslide, ID and length (L) are provided. For the full list of the landslides catalogued in this work, see Supplementary Table T1.

https://doi.org/10.5194/esurf-2023-13
Preprint. Discussion started: 15 May 2023

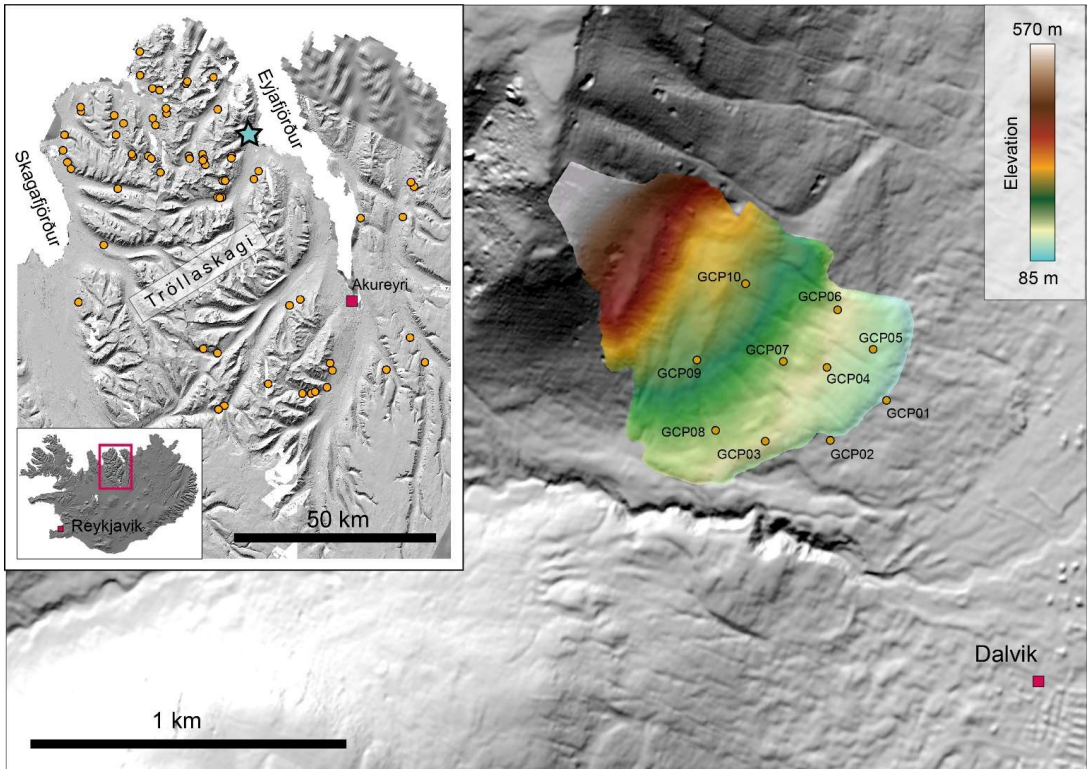

Figure 4: The Dalvík landslide in the Tröllaskagi peninsula. The landslide is located near the town of Dalvík. The landslide is ID 47 in the Icelandic catalogue of long runout landslides with longitudinal ridges that we compiled in this work. The figure shows in colour the DEM generated from drone imagery overlain on a hillshaded render of the ArcticDEM and the points indicate the location of 10 GCPs used to georeference the DEM. The inset shows the location of the Dalvík landslide in Tröllaskagi peninsula (blue star) along with the other landslides in this work (orange dots), showing that it is the Icelandic region with the highest landslide density. The location of the Tröllaskagi peninsula within Iceland is shown in the bottom left corner of the inset with red box. The inset uses as a basemap the hillshaded ArcticDEM.

https://doi.org/10.5194/esurf-2023-13
Preprint. Discussion started: 15 May 2023

Earth Surface Dynamics
Discussions
Open Access
EGU

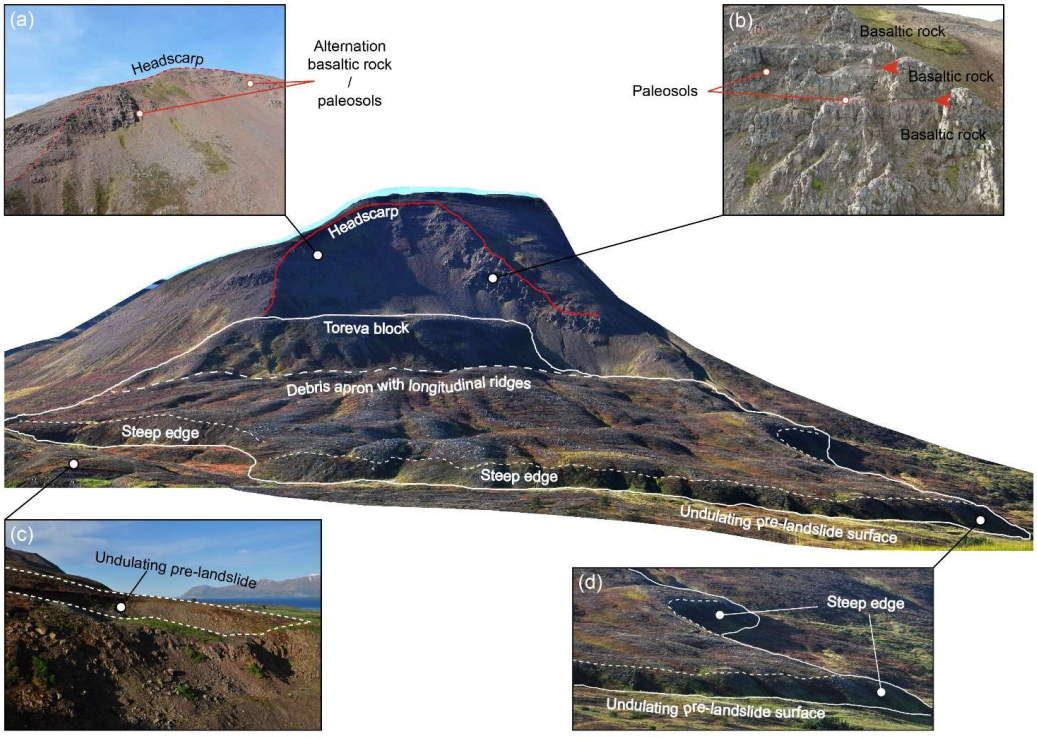

Figure 5: The Dalvík landslide. The image in the centre shows a perspective view of the drone photomosaic of the Dalvík landslide. Annotations highlight the main morphological features and structures. Panel a) and b) are photos acquired by drone showing details of the rock formations that characterise the headscarp. Panel c) shows an outcrop of the unsorted sediments that form the undulating pre-landslide surface over which the Dalvík landslide is found. Panel d) shows a closer view of the 15-25 m high, steep termination of the landslide deposit.

https://doi.org/10.5194/esurf-2023-13
Preprint. Discussion started: 15 May 2023

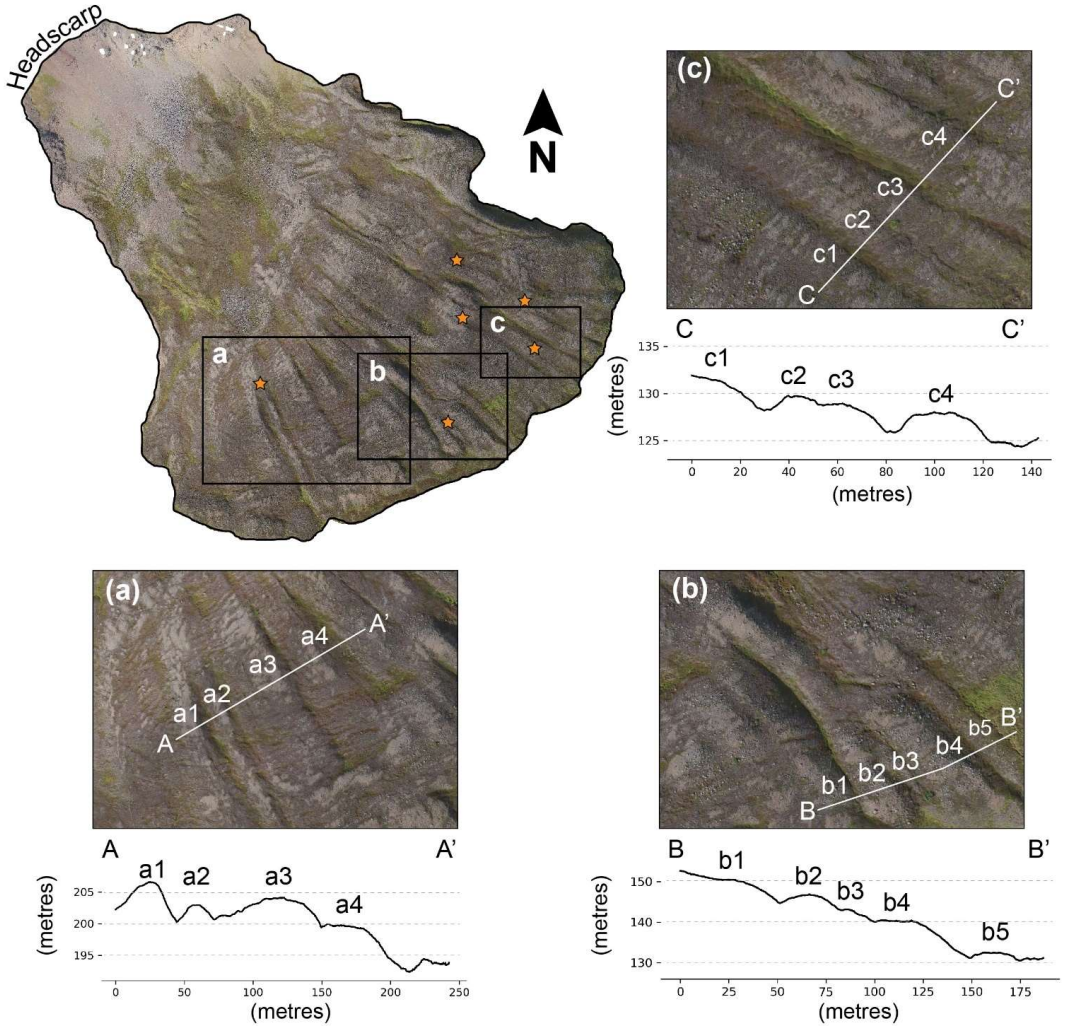

Figure 6: Morphology of longitudinal ridges in Dalvik landslide. The image shows the high resolution orthoimage of the Dalvík landslide generated from drone-acquired photos. The orthoimage provides complete view of the extent of longitudinal ridges over the landslide deposit. Panels a), b) and c) show close-up views of longitudinal ridges, whose morphology is shown by topographic profiles extracted from the profiles (A-A', B-B', and C-C', respectively) and the annotations a1, a2, etc indicate corresponding ridges in the images and profiles. The stars show locations where longitudinal ridges bifurcate, resulting in the development of two ridges from a parent ridge.

https://doi.org/10.5194/esurf-2023-13
Preprint. Discussion started: 15 May 2023

Earth Surface Dynamics Discussions
Open Access
EGU

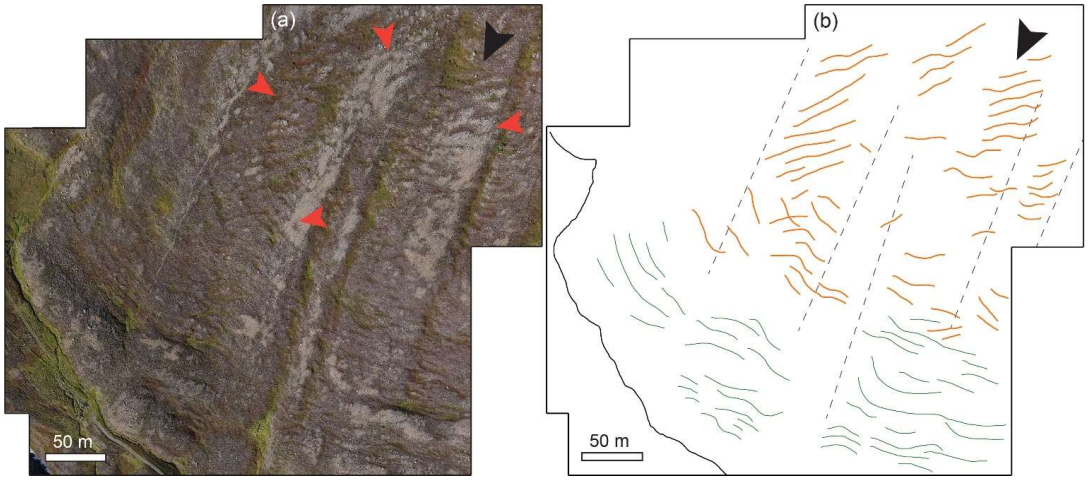

Figure 7: En-echelon structures found superposing longitudinal ridges of the Dalvík landslide. Panel a) Drone-acquired image mosaic of the SW terminal part of the Dalvík landslide. Panel b) shows digitised en-echelon features observed on the longitudinal ridges in panel a). Orange lines represent the linear structures that are oblique to the direction of the ridges, which are shown with dashed black lines. Green lines represent the linear structures that are transverse to the direction of the ridges. This map shows how the transition from oblique-to-transverse occurs towards the terminal part of the deposit. Black arrowheads show the direction of movement of the landslide; red arrowheads show locations where en-echelon linear structures are found superposing longitudinal ridges.

https://doi.org/10.5194/esurf-2023-13
Preprint. Discussion started: 15 May 2023

Earth Surface Dynamics Discussions
Open Access
EGU

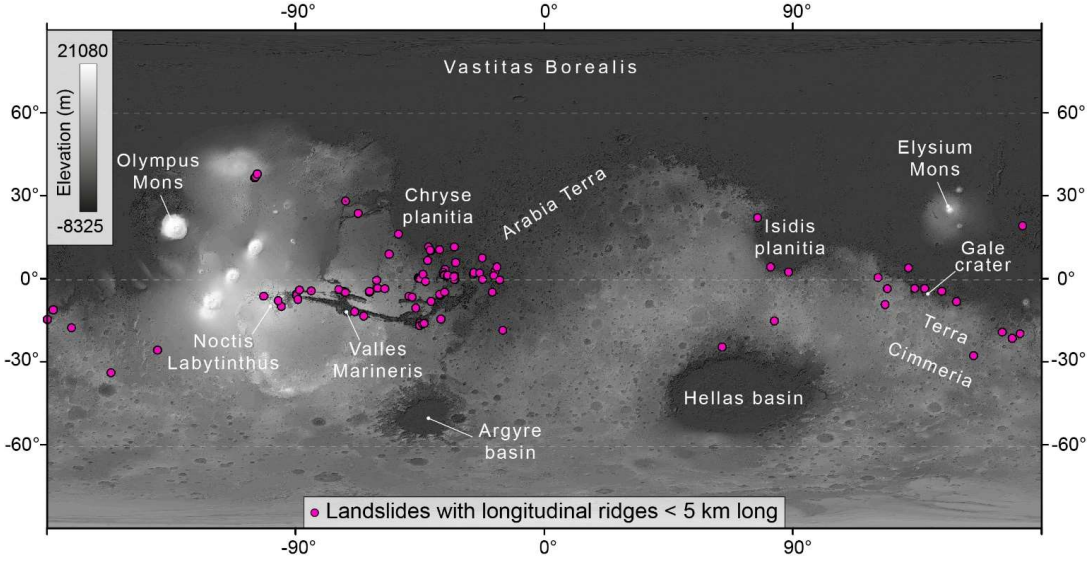

Figure 8: Distribution of long runout landslides (less than 5 km long) with longitudinal ridges on Mars. The pink dots represent the locations of 112 long runout landslides with longitudinal ridges, which geographic coordinates given in Supplementary Table T3. Base map is a greyscale render of the HRSC MOLA-blended global digital elevation model (200 m/px resolution). Some examples of the landslide deposits included in this catalogue are shown in Figure 7.

https://doi.org/10.5194/esurf-2023-13
Preprint. Discussion started: 15 May 2023

Earth Surface Dynamics Discussions
Open Access
EGU

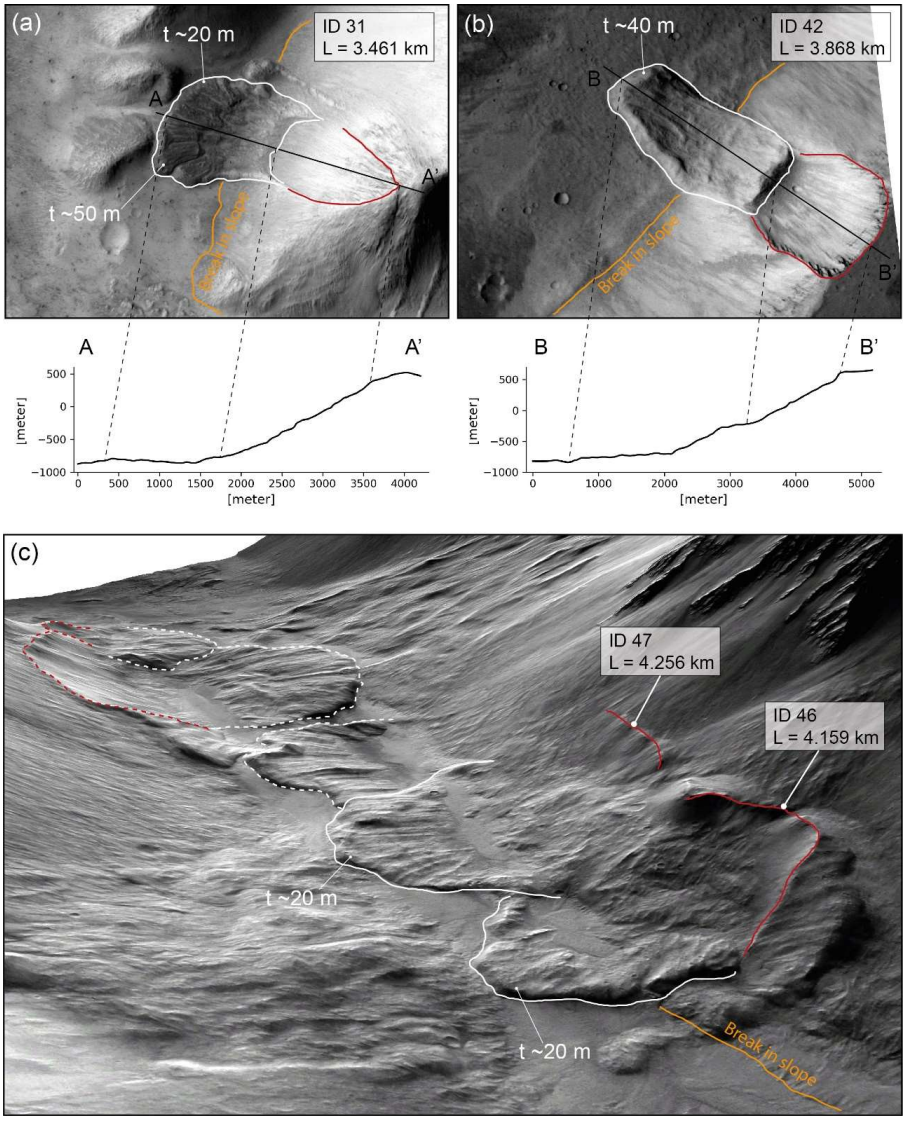

Figure 9: Martian long runout landslides with longitudinal ridges. Panels a) and b) show top-views of landslide ID 31 (CTX image D16_033578_1752_XN_04S084W) and landslide ID 42 (CTX image D21_035252_2083_XN_28N072W), and their longitudinal topographic profiles; in both panels, North is up. Panel c) is an oblique view of a cluster of landslides with longitudinal ridges (J16_050944_1665_XN_13S065W). Red lines show headscarps; white lines show landslide deposits (dashed red and white lines are for landslides not included in the catalogue because either too long (> 5 km) or missing the headscarp); orange lines show the base of the slope. In each panel, the landslide ID, lengths, and thickness (t) values at the frontal edge are provided.

https://doi.org/10.5194/esurf-2023-13
Preprint. Discussion started: 15 May 2023

Earth Surface Dynamics Discussions
Open Access
EGU

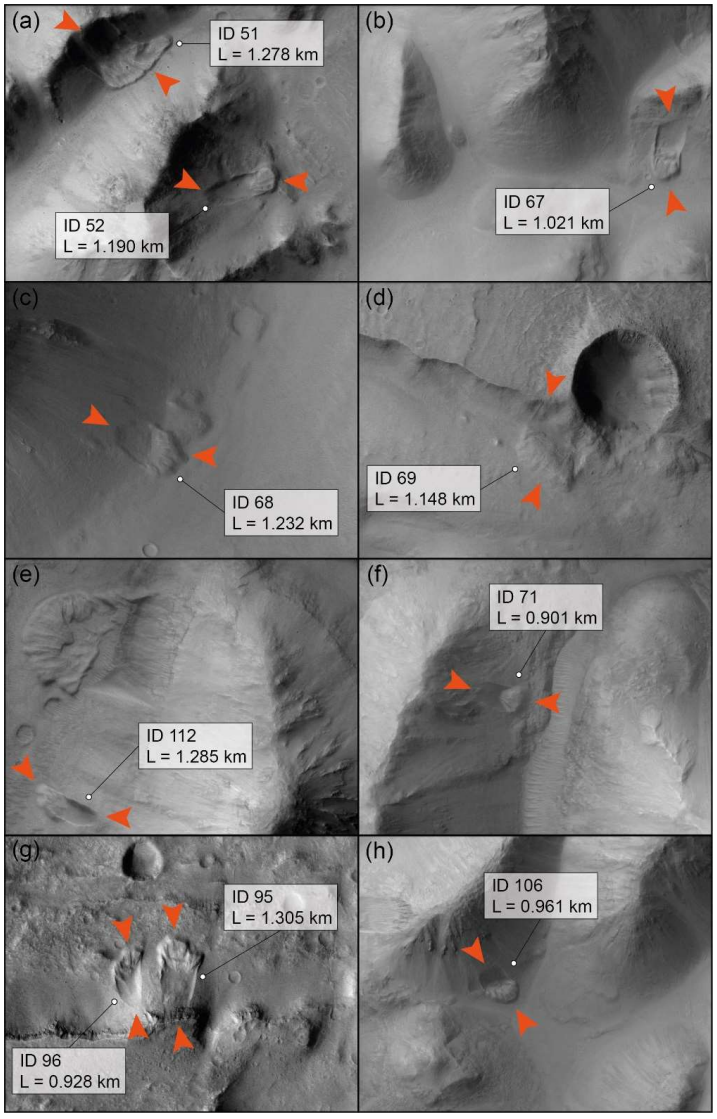

630 **Figure 10: Examples of martian long runout landslides less than 5 km long that exhibit longitudinal ridges.** The orange arrowheads show the approximation location of the headscarp and of the toe of the landslides. For each landslide, ID and length are provided. For the full list of the landslides catalogued in this work, see Supplementary Table T3. In all panels, North is up. a) CTX image P16_007244_1796_XN_00S045W; b) CTX image P19_008417_1807_XN_00N036W; c) CTX image P05_002800_1814_XI_01N035W; d) CTX image P02_002022_1801_XN_00N035W; e) CTX image P16_007349_1831_XN_03N032W; f) CTX image

https://doi.org/10.5194/esurf-2023-13
Preprint. Discussion started: 15 May 2023

Earth Surface Dynamics Discussions
Open Access
EGU

635 B19_017001_1789_XN_01S032W; g) CTX image P04_002642_1717_XI_08S041W; h) CTX image B19_017001_1789_XN_01S032W. Image credit: NASA/JPL/MSSS

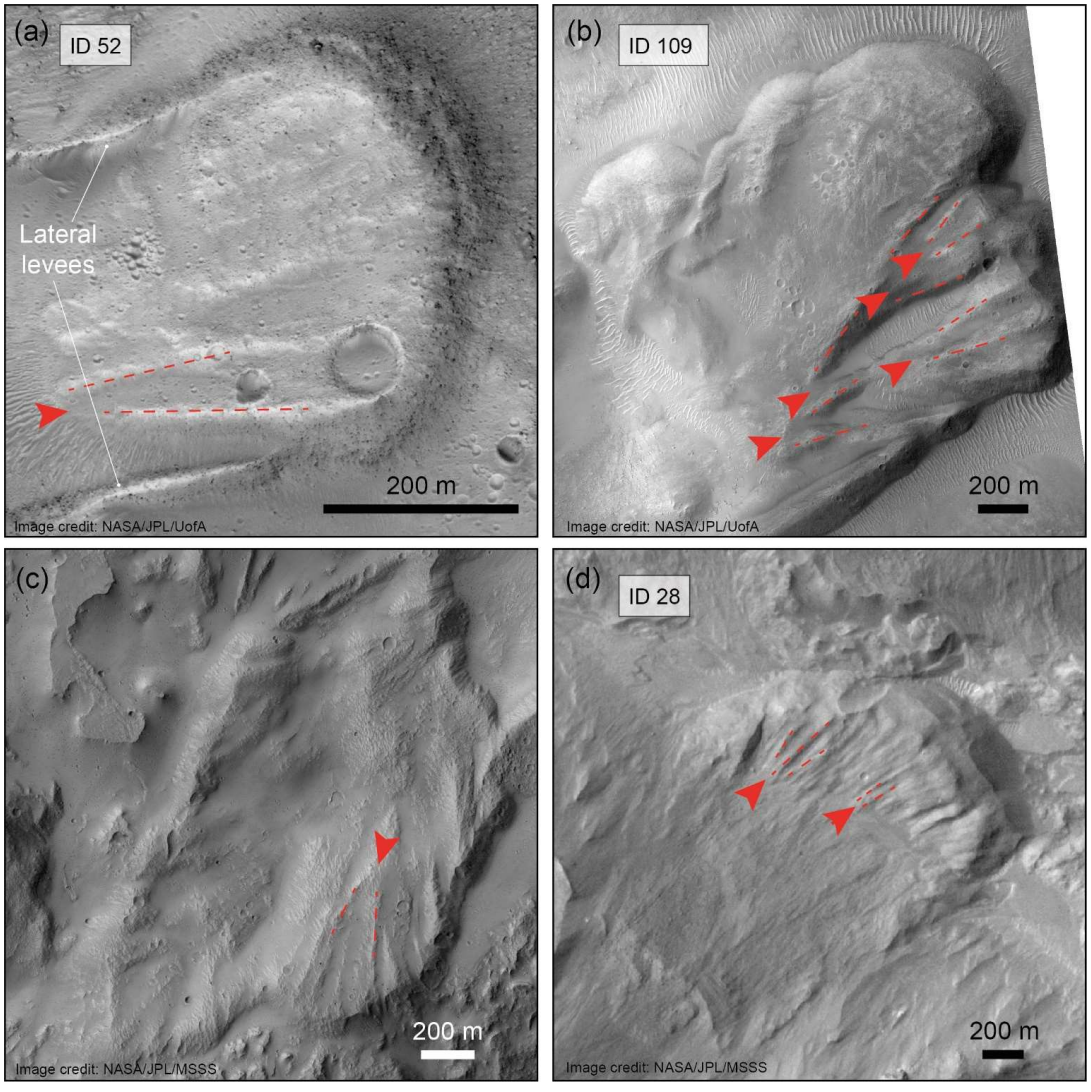

Figure 11: Behaviour of longitudinal ridges in small-scale (< 5 km long) martian long runout landslides. The red arrowheads show the locations where longitudinal ridges bifurcate, resulting in the development of two ridges from a parent ridge. Dashed red lines show the
640 orientation of longitudinal ridges. Panel a), b), and d) show examples of landslides included in this work and whose number ID is provided in the figure (HiRISE images: ESP_040790_1805, ESP_070830_1795 and ESP_026497_1755, respectively. Image credit:

https://doi.org/10.5194/esurf-2023-13
Preprint. Discussion started: 15 May 2023

Earth Surface Dynamics Discussions
Open Access
EGU

NASA/JPL/UofA). Panel c) shows an example of bifurcating longitudinal ridges in a landslide not included in the list presented in this work, as its length is slightly more than 5 km (CTX image: P01_001337_1757_XN_04S063W. Image credit: NASA/JPL/MSSS). In all panels, North is up.

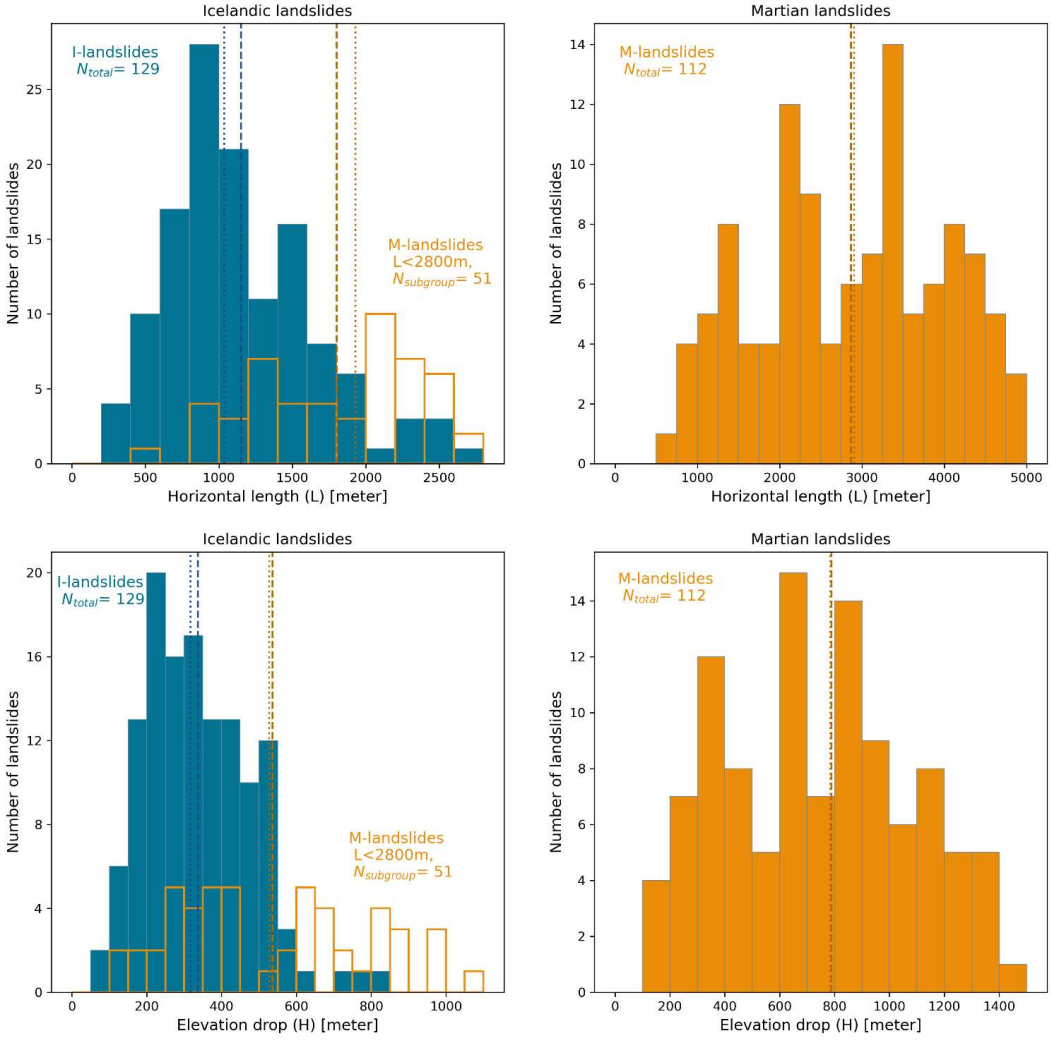

645

Figure 12: Morphometric results. The data in 'sea blue' colour represent the Icelandic landslide population. The data in 'gold' colour represent the martian landslides less than 5 km long. Top panels show the distribution of landslide lengths. The lower panels show the distribution of landslide elevation drops. In the panels showing Icelandic landslides, the data relative to the subgroup of the martian

https://doi.org/10.5194/esurf-2023-13
Preprint. Discussion started: 15 May 2023

Earth Surface Dynamics Discussions
Open Access
EGU

landslides with maximum length less than or equal to the maximum length of the Icelandic landslides are also plotted. Dashed lines represent the mean and dotted lines represent the median.

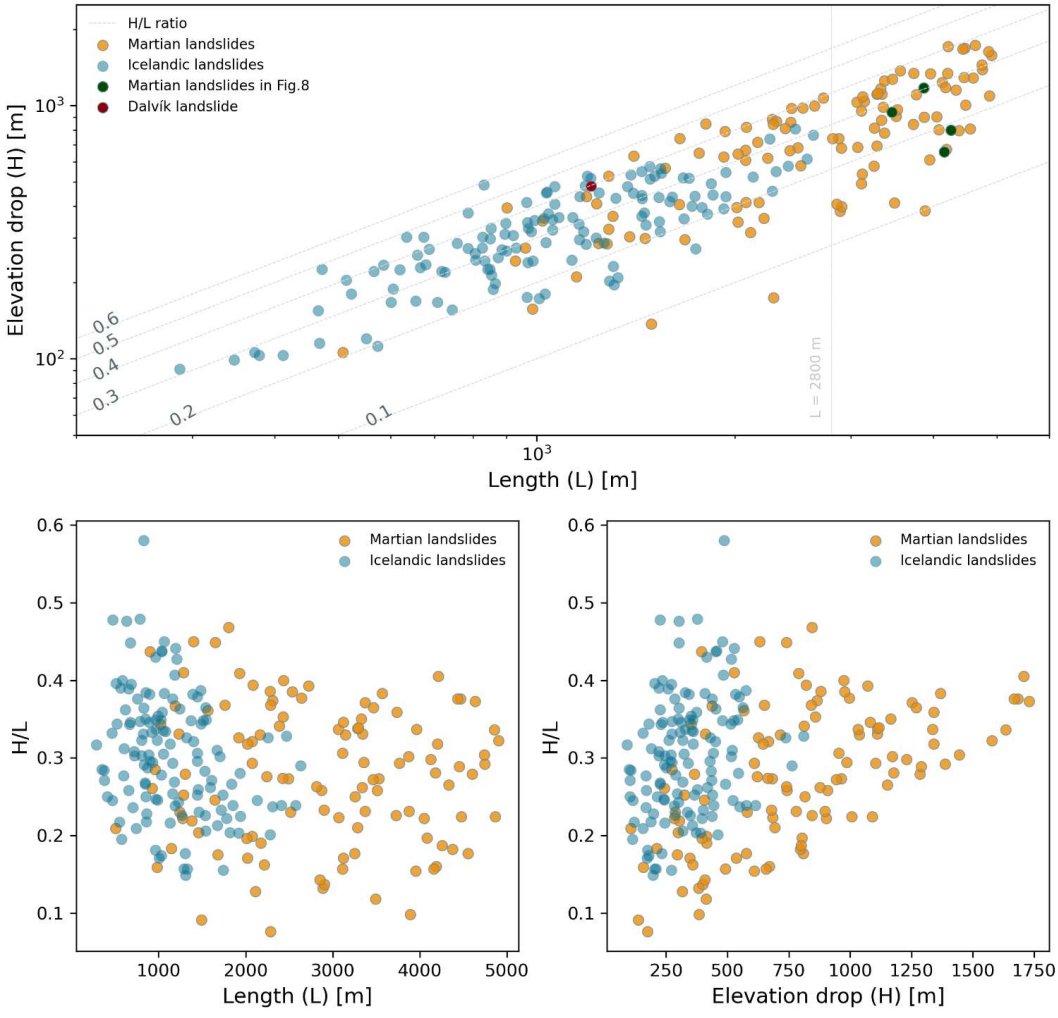

Figure 13: H/L ratio. In this plot the elevation drop (H) is plotted against the horizontal length (L) to visually represent the H/L ratios that characterise the landslides compiled in this study. The dashed grey lines represent constant H/L ratios, whose values are given at the left-hand side of each line. The light grey vertical line shows the value of L = 2800 m, which corresponds to the maximum length of the martian landslide subgroup.

https://doi.org/10.5194/esurf-2023-13
Preprint. Discussion started: 15 May 2023

Earth Surface Dynamics Discussions
Open Access
EGU

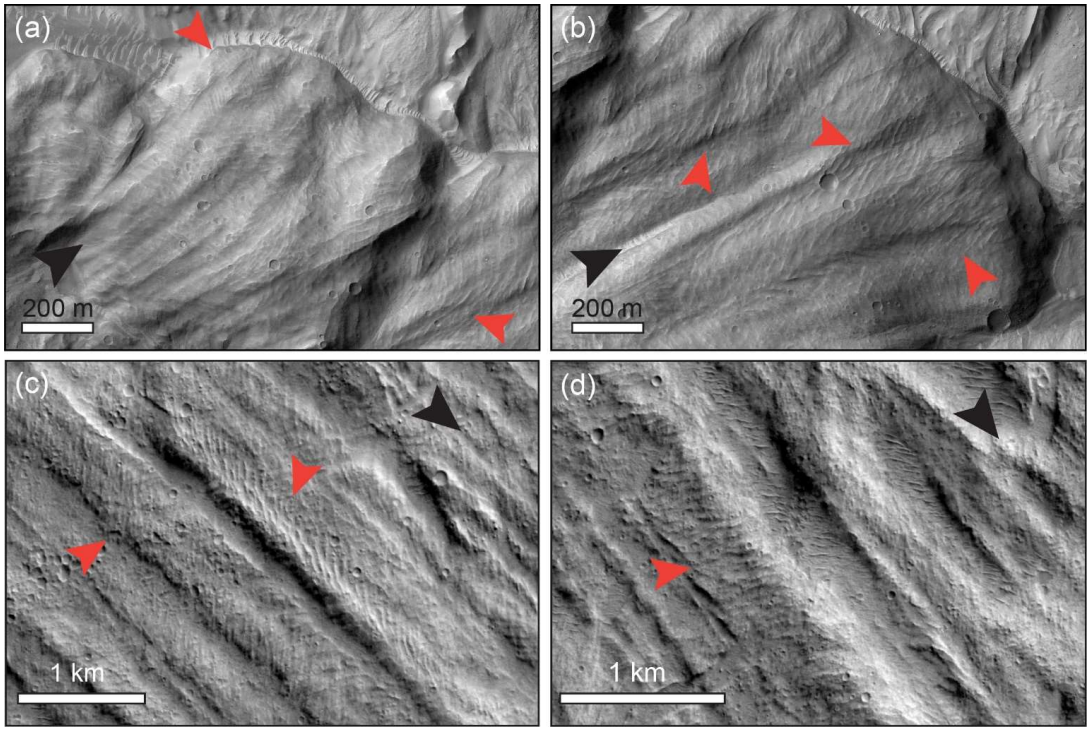

660 **Figure 14: En-echelon structures found superposing longitudinal ridges in martian long runout landslides.** Panels a) and b) show examples of linear structures superposed on longitudinal ridges in an 8-km-long landslide on Mars (HiRISE image: ESP_016778_1750). Panels c) and d) show examples from the 63-km-long Coprates Labes landslide deposit on Mars (CTX image: P20_008906_1685_XN_11S067W). In all panels, black arrowheads show the direction of movement of the landslides; red arrowheads show locations where en-echelon linear structures are found superposing longitudinal ridges (note that these are examples and the 665 structures are found ubiquitously on the deposits).